5. Tracking Detectors

5.1 Momentum reconstruction in a magnetic field

5.2 Magnetic spectrometers

5.3 Multi-wire proportional chambers

5.4 Drift chambers

5.5 Time projection chambers

5.6 Microstrip gas chambers

Silicon-based tracking detectors are discussed in Chapter 6
(together with impact parameter resolutions)

5.1 Introduction: The motivation for tracking detectors

- Main purpose: measure coordinates of charged particles with high precision in a magnetic field

- Measure the curvature → momentum
  (or more general: five track parameters)

- Curvature measurement requires the reconstruction of track patterns in an ensemble of measured hits in detectors
  → pattern recognition (reconstruction software)

  hits → coordinates → tracks → momentum

- Additional tasks: vertex reconstruction
  extrapolate tracks back to their origin
  → primary vertex at the interaction point or secondary vertex

- Determination of impact parameter w.r.t. primary vertex → lifetime tags (b-tagging)

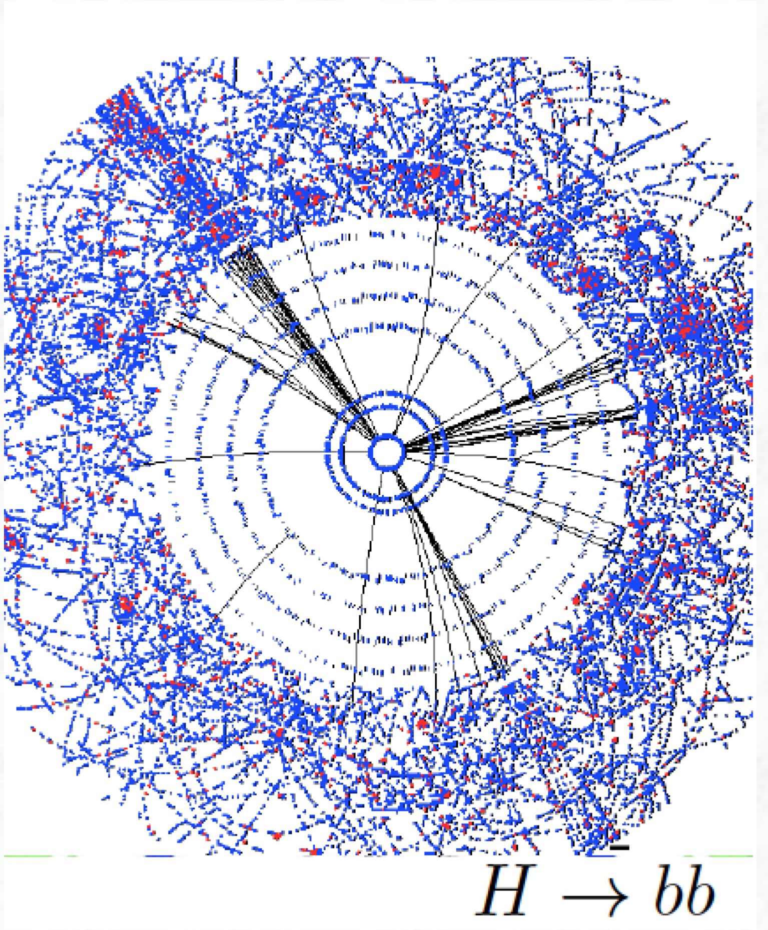

Motivation for tracking detectors (cont.)

- Recognition and reconstruction of charged particle trajectories (tracks)
- Measurement of momentum (and sign of charge) in a magnetic field

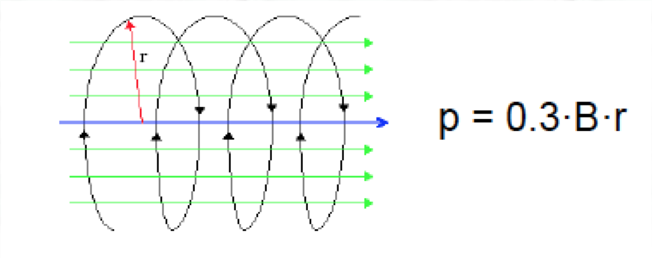

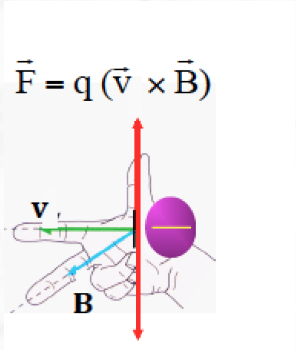

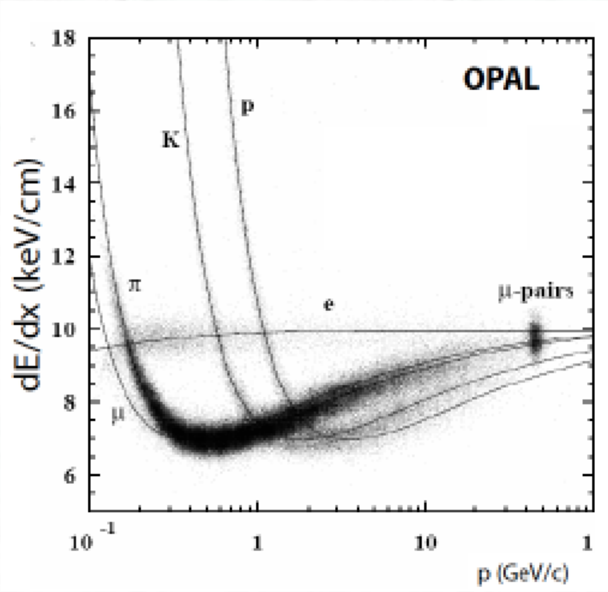

- Vertex reconstruction and lifetime "tag" (via secondary verteices)

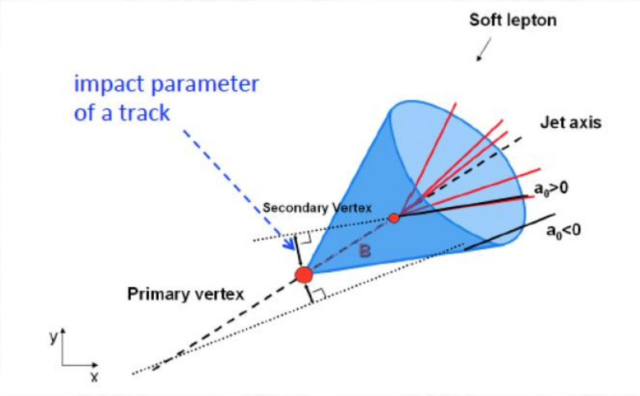

- dE/dx measurement (requires measurement of charge) and contribution to particle ID

Momentum reconstruction

- Equation of motion (general form): $\vec{F} = m \cdot \gamma \cdot \vec{a} = q(\vec{v} \times \vec{B})$

  2nd order differential equation: $\ddot{\vec{x}} = \dfrac{q}{m \cdot \gamma} \dot{\vec{x}} \times \vec{B}(x)$

- There are in general two types of experimental setups:

  (i) Fixed target experiments

  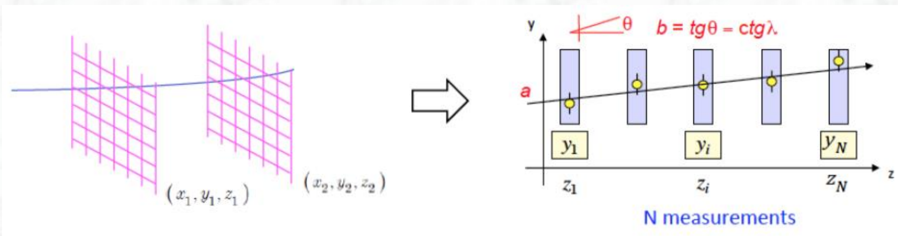

  Measured coordinates: $x(z_i)$, $y(z_i)$

  (ii) Collider experiments

  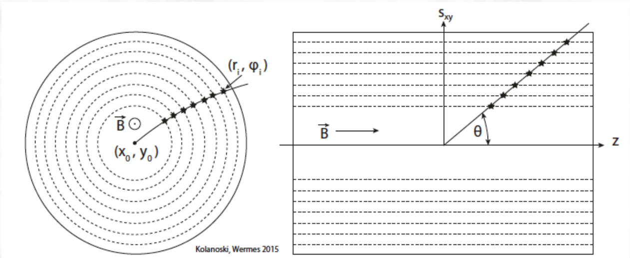

  $\phi(r_i)$, $z(r_i)$

- General equation (fixed target approach): $\dfrac{dx}{dt} \rightarrow \dfrac{dx}{dz} = x' \quad \dfrac{dy}{dz} = y'$

$$p \cdot y''(z) = \sqrt{1 + y'(z)^2 + x'(z)^2}\,\left\{ B_z x' + B_y y' x' - B_x (1 + y'^2) \right\}$$

$$p \cdot x''(z) = \sqrt{1 + y'(z)^2 + x'(z)^2}\,\left\{ -B_z y' - B_x y'z' + B_y (1 + x'^2) \right\}$$

Solution has four integration constants + momentum p → five parameters
→ at least five independent coordinate measurements (3 space points) needed

Case of a homogenous magnetic field, e.g. solenoid field in collider experiments

$$\vec{F} = \dot{\vec{p}} = q\left(\vec{v} \times \vec{B}\right) \quad \Rightarrow \quad \boxed{\dot{\vec{v}} = \frac{q}{\gamma m}\left(\vec{v} \times \vec{B}\right)}$$

diff. equation

- solution is a rotating vector $\vec{v}_T$ in plane perpendicular to $\vec{B}$ $\quad \vec{v}_{||}$ is unchanged

$$B_1 = B_2 = 0, \; B_3 = B > 0$$

$$\omega_B = \frac{|q|\,B}{\gamma m}$$

$$\Rightarrow$$

$$\begin{aligned} v_1 &= v_T \cos(\eta\,\omega_B\,t + \psi) \\ v_2 &= -v_T \sin(\eta\,\omega_B\,t + \psi) \\ v_3 &= v_3 \end{aligned}$$

$$\eta = \frac{q}{|q|}$$

equations also hold relativistically $\omega_B = \omega_B(\gamma); E = \gamma m$

- integration yields spatial trajectory

$$\begin{aligned} x_1 &= \frac{v_T}{\eta\,\omega_B} \sin(\eta\,\omega_B\,t + \psi) + x_{10} \\ x_2 &= \frac{v_T}{\eta\,\omega_B} \cos(\eta\,\omega_B\,t + \psi) + x_{20} \\ x_3 &= v_3\,t + x_{30} \end{aligned}$$

curvature radius

$$\boxed{R} = \sqrt{(x_1 - x_{10})^2 + (x_2 - x_{20})^2} = \frac{v_T}{\omega_B} = \frac{\gamma\,m\,v_T}{|q|\,B} = \boxed{\frac{p_T}{|q|\,B}}$$

The Helix…. as seen in an experiment

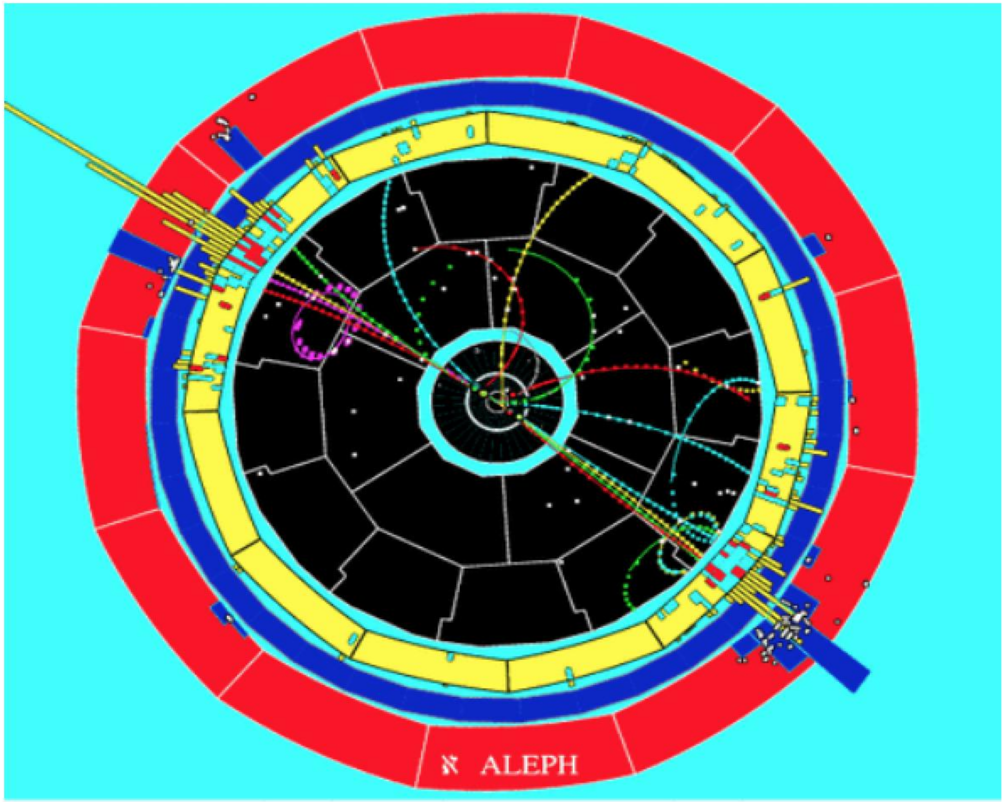

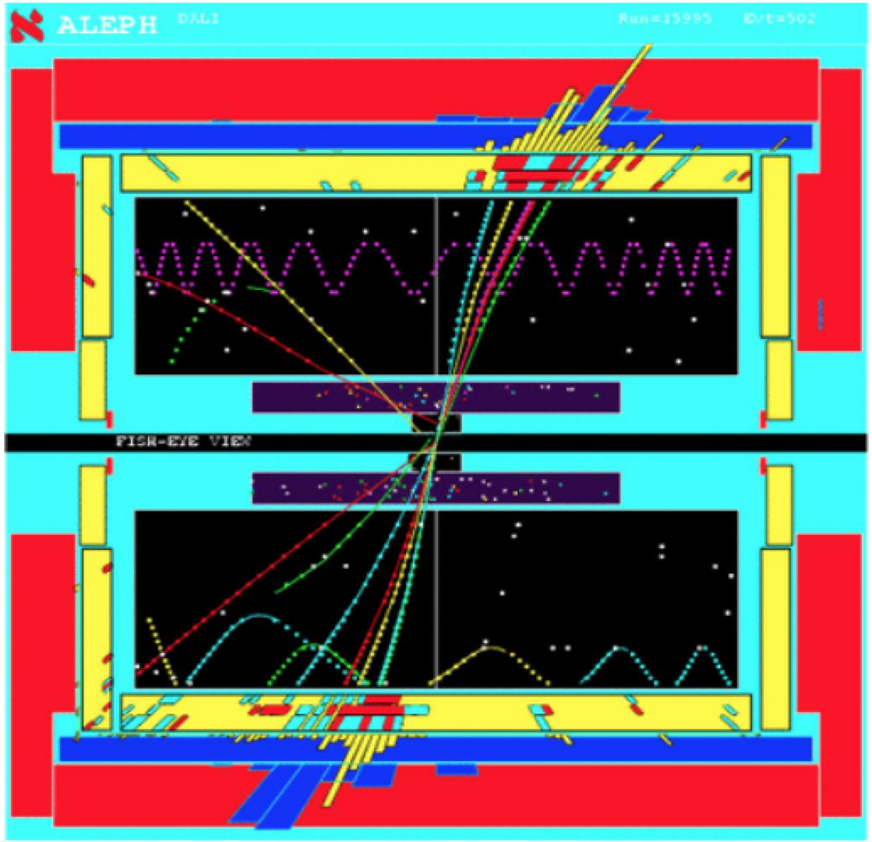

Event from the ALEPH experiment at LEP

- For low momenta y is a periodic function of z
- For high momenta y is a linear function of z

The Helix as explicit track model:

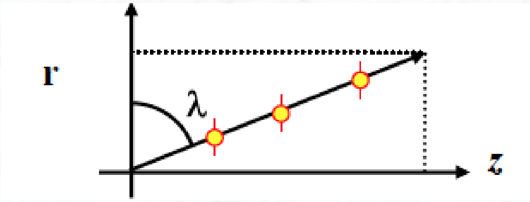

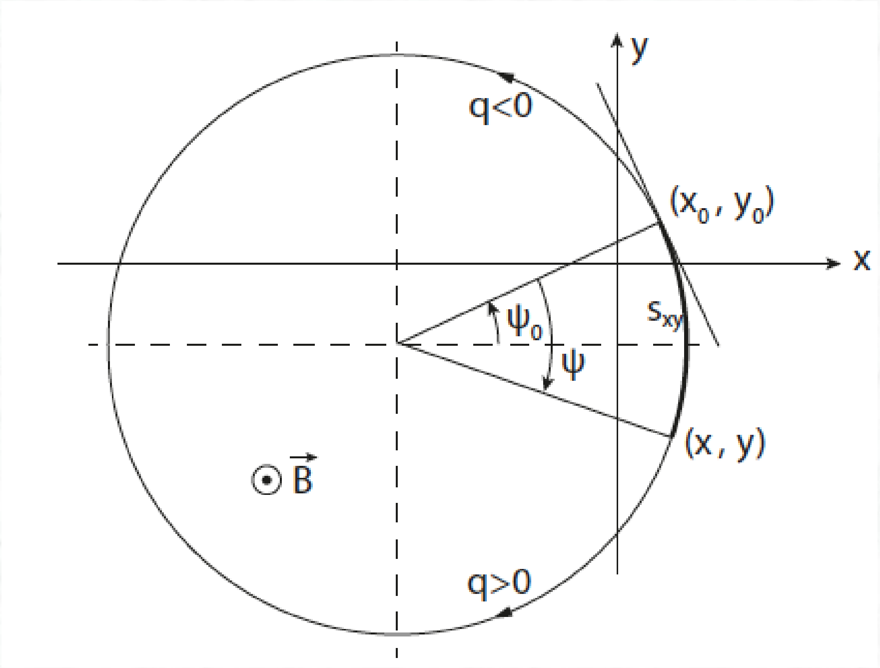

$$x = x_0 + R\left(\cos(\psi_0 - \eta\psi) - \cos\psi_0\right)$$
$$y = y_0 + R\left(\sin(\psi_0 - \eta\psi) - \sin\psi_0\right)$$
$$z = z_0 + \frac{\psi R}{\tan\theta}.$$

The representation of the circular projection can be expanded for large R
→ parabolic equation

$$y = y_0 + \sqrt{R^2 - (x - x_0)^2}$$

$$y = y_0 + R\left(1 - \frac{(x - x_0)^2}{2R^2} + \dots\right) = \left(y_0 + R - \frac{x_0}{2R^2}\right) + \frac{x_0}{R}x - \frac{1}{2R}x^2 + \dots$$

$\approx a + bx + cx^2$

What do we need to do ?

- **Once we have measured the transverse momentum and the dip angle the total momentum is**

$$P = \frac{P_\perp}{\cos\lambda} = \frac{0.3BR}{\cos\lambda}$$

- **The error on the momentum is given by the measurement errors on the curvature radius R and the dip angle λ**

$$\frac{\partial P}{\partial R} = \frac{P_\perp}{R}$$

$$\frac{\partial P}{\partial \lambda} = -P_\perp \tan\lambda$$

$$\boxed{\left(\frac{\Delta P}{P}\right)^2 = \left(\frac{\Delta R}{R}\right)^2 + (\tan\lambda\Delta\lambda)^2}$$

relative error (%)

- **We need to study (for solenoid magnets)**
  - the error on the radius measured in the bending plane r - ϕ
  - the error on the dip angle in the r - z plane
- **… and also**
  - The contribution of multiple scattering to the momentum resolution
- **Comment:**
  - in a hadron collider like LHC the main emphasis is on transverse momentum measurement
  - elementary processes take place among partons that are not at rest in the laboratory frame
  - → use momentum conservation only in the transverse plane

Estimation of Track parameters and their uncertainties

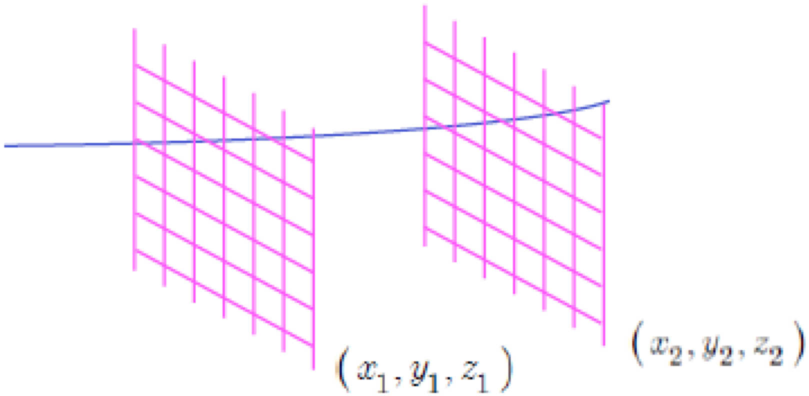

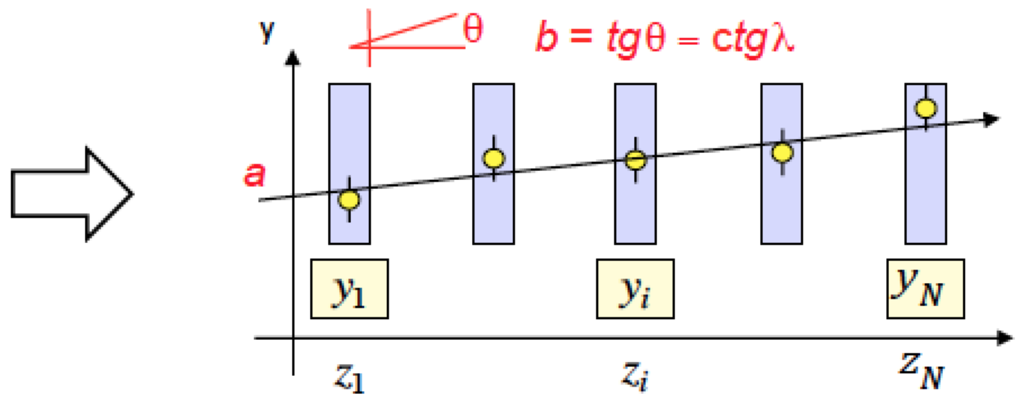

N measurements

χ^2 minimization of S (see lecture on Statistical Methods)

$$S = \sum_{i=1}^{N}\sum_{j=1}^{N}(\xi_i^{meas} - \xi_i^{fit})\, V_{y,ij}^{-1}\, (\xi_j^{meas} - \xi_j^{fit}) \;= \sum_{i=1}^{N} \frac{(\xi_i^{\mathrm{mess}} - \xi_i^{fit}(\theta))^2}{\sigma_i^2}$$

if V is diagonal

covariance matrix

General track fit in matrix formalism (x-y space)

- **f be a linear function of the parameters θ_i:** $f(x|\theta) = \theta_1 f_1(x) + \ldots + \theta_m f_m(x) = \sum_{j=1}^{m} \theta_j f_j(x)$
- **then the expectation values for the measurement points at positions x_i are:**

$$\eta_i = \theta_1 f_1(x_i) + \ldots + \theta_m f_m(x_i) = \sum_{j=1}^{m} \theta_j f_j(x_i) = \sum_{j=1}^{m} H_{ij} \theta_j$$

n x m matrix

- **the minimization requirement then reads:**

$$\Rightarrow \boxed{S = (\vec{y} - H\theta)^T V_y^{-1} (\vec{y} - H\theta) \longrightarrow \text{min}}$$

with solution $\hat{\theta} = \underbrace{\left(H^T V_y^{-1} H\right)^{-1} H^T V_y^{-1}}_{=:\,A} \vec{y} = A\vec{y} \quad \Rightarrow \quad \boxed{\hat{y} = \sum_{j=1}^{m} \hat{\theta}_j f_j(x)}$ best coord. estimate for given x

and errors $V_\theta = A V_y A^T = \left(H^T V_y^{-1} H\right)^{-1}$ (error propagation = linear trafo of V_y)

$$\Rightarrow \sigma_y^2 = \sum_{i=1}^{m} \sum_{j=1}^{m} \frac{\partial y}{\partial \theta_i} \frac{\partial y}{\partial \theta_j} V_{\theta,ij} = \boxed{\sum_{i=1}^{m} \sum_{j=1}^{m} f_i(x) f_j(x) V_{\theta,ij}}$$

error of best fit coordinate

Application to a straight line:

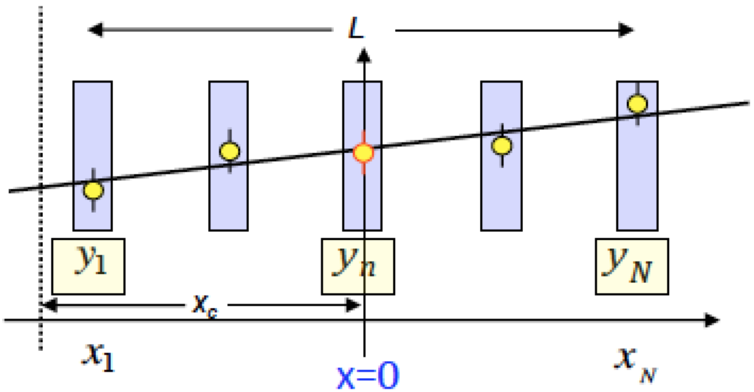

$$f_1(x) = 1,\ f_2(x) = x$$

$$\theta_1 = a,\ \theta_2 = b$$

N measurements

$$\Rightarrow \quad y = f(x|\theta) = a + b\,x$$

fit $\quad \Rightarrow \quad \hat{y} = \sum_{j=1}^{m} \hat{\theta}_j\, f_j(x)$

best estimate of y for a given x

with errors (on parameters)

$$V_\theta = A\,V_y\,A^T = \left(H^T\,V_y^{-1}\,H\right)^{-1} \quad \Rightarrow \quad \begin{cases} \sigma_a^2 = \dfrac{\sigma^2}{N} \\ \boxed{\sigma_b^2 = \dfrac{\sigma^2}{N}\dfrac{12(N-1)}{(N+1)\,L^2}} \\ \sigma_{ab} = 0 \end{cases}$$

cf. choice of coord. system

... and errors on position estimates

$$\sigma_y^2 = \sum_{i=1}^{m}\sum_{j=1}^{m} \frac{\partial y}{\partial \theta_i}\frac{\partial y}{\partial \theta_j} V_{\theta,ij} \quad \Rightarrow \quad \boxed{\sigma_y^2 = \sigma_a^2 + x_0^2\,\sigma_b^2 = \frac{\sigma^2}{N} + \frac{\sigma^2}{N}\frac{12(N-1)}{(N+1)}\frac{x_0^2}{L^2}}$$

x_0 is a specifically chosen x-value

Application to a linearized circle:

$$y = y_0 + \sqrt{R^2 - (x - x_0)^2}$$

$$\Rightarrow y \approx a \ + \ bx \ + \ \frac{1}{2}cx^2$$

errors

$$V_\theta = A\,V_y\,A^T = \left(H^T\,V_y^{-1}\,H\right)^{-1} \quad \Rightarrow \quad \begin{cases} \sigma_a^2 = \sigma^2 \dfrac{3N^2 - 7}{4(N-2)N(N+2)} \\ \sigma_b^2 = \dfrac{\sigma^2}{L^2}\dfrac{12(N-1)}{N(N+1)} \\ \boxed{\sigma_c^2 = \dfrac{\sigma^2}{L^4}\dfrac{720(N-1)^3}{(N-2)N(N+1)(N+2)}} \\ \sigma_{ab} = \sigma_{bc} = 0 \\ \sigma_{ac} = \dfrac{\sigma^2}{L^2}\dfrac{30N}{(N-2)(N+2)} \end{cases}$$

$$\sigma_y^2 = \sum_{i=1}^{m}\sum_{j=1}^{m} \frac{\partial y}{\partial \theta_i}\frac{\partial y}{\partial \theta_j} V_{\theta,ij}$$

$$\Rightarrow \quad \sigma_y^2 = \sigma_a^2 + x_0^2\,\sigma_b^2 + \frac{1}{4}x_0^4\,\sigma_c^2 + x_0^2\,\sigma_{ac}$$

$$\boxed{= \frac{\sigma^2}{N}\left(1 + \frac{x_0^2}{L^2}\frac{12(N-1)}{(N+1)} + \frac{x_0^4}{L^4}\frac{180(N-1)^3}{(N-2)(N+1)(N+2)} + \frac{x_0^2}{L^2}\frac{30N^2}{(N-2)(N+2)}\right)}$$

x_0 is a specifically chosen x-value

Important application: A solenoidal magnetic field

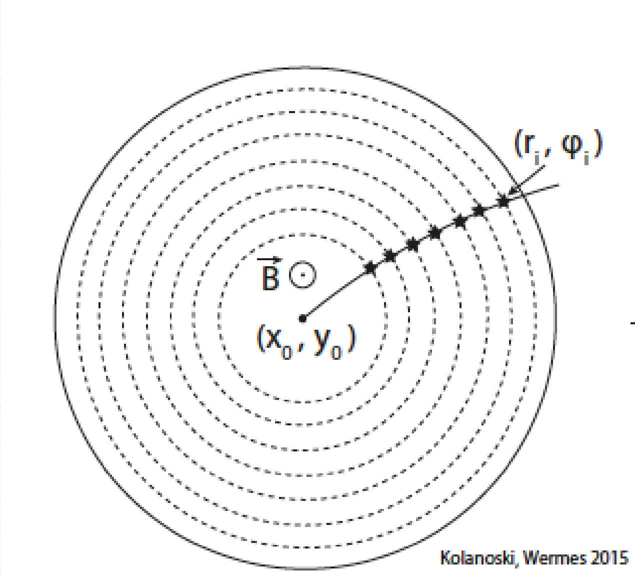

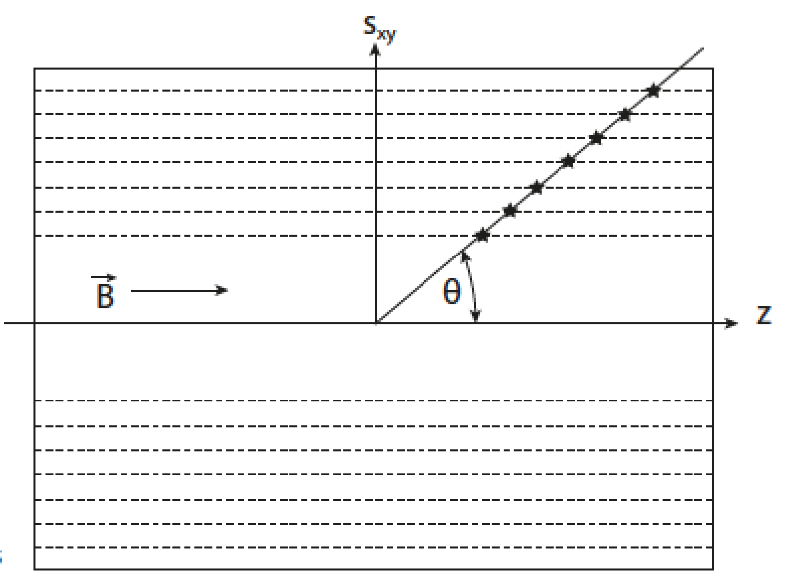

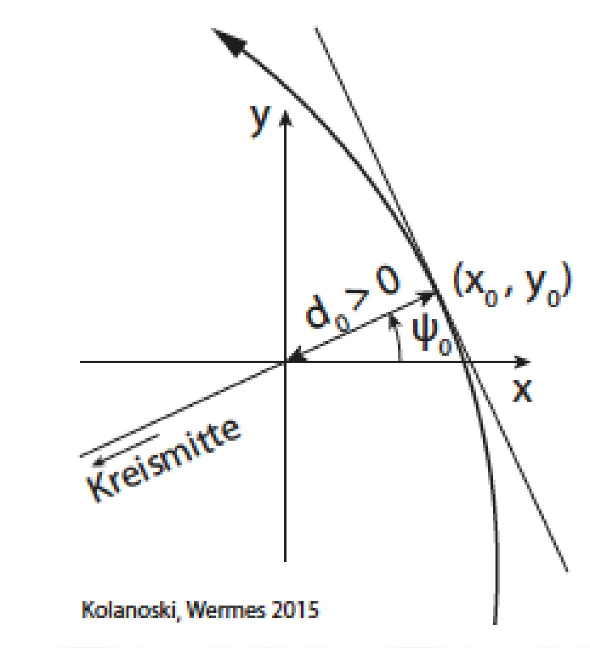

beam position can often be used as additional constraint

Measure: (r_i, ϕ_i) or (r_i, ϕ_i, z_i)

In general a helix model with the following five parameters is used:

$$\kappa = \pm 1/R,\ \psi_0,\ d_0,\ \theta,\ z_0$$

$x_0 = d_0 \cos \psi_0$, and $y_0 = d_0 \sin \psi_0$

The precision of a measurement of the momentum in a homogeneous magnetic field is determined by the precision of the sagitta measurement (s)

$$p_T = |q|\, B\, R = \frac{q\,B}{\kappa}$$

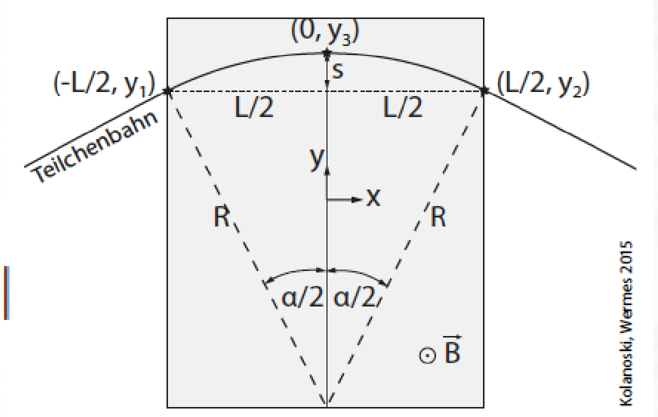

Relation between R and s:

$$\frac{R-s}{R} = \cos\frac{\alpha}{2} \approx 1 - \frac{\alpha^2}{8}$$
$$\frac{L}{2\,R} = \sin\frac{\alpha}{2} \approx \frac{\alpha}{2}$$

$\rightarrow$ $$s = \frac{R\,\alpha^2}{8} = \frac{1}{8}\frac{L^2}{R} = \frac{1}{8}L^2\,|\kappa|$$

→ the precision of the momentum measurement depends on the precision of the sagitta measurement:

$$\boxed{\sigma_\kappa = \frac{8}{L^2}\,\sigma_s}$$

For three distinct points (see drawing):

$$s = y_3 - \frac{y_1 + y_2}{2} \;\rightarrow\; \sigma_s = \sqrt{\sigma^2_{\mathrm{mess}} + \frac{1}{4}\,2\,\sigma^2_{\mathrm{mess}}} = \sqrt{\frac{3}{2}}\,\sigma_{\mathrm{mess}} \;\rightarrow\; \boxed{\sigma_\kappa = \frac{\sqrt{96}}{L^2}\sigma_{mess}}$$

For N equidistant measurements one obtains from the linearized circle approximation:

$$\boxed{\sigma_\kappa = \frac{\sigma_{\mathrm{mess}}}{L^2}\sqrt{\frac{720(N-1)^3}{(N-2)N(N+1)(N+2)}}} \; \boxed{\approx \frac{\sigma_{\mathrm{mess}}}{L^2}\sqrt{\frac{720}{N+4}}}$$

From the measurement on the curvature to the p_T measurement:

$$p_T = |q|\,B\,R = \frac{q\,B}{\kappa}$$

For the uncertainty on p_T one obtains:

$$\sigma_{p_T} = \frac{p_T^2}{|q|\,B}\sigma_\kappa = \frac{p_T^2}{0.3\,|z|\,B}\sigma_\kappa$$

→ for the relative uncertainty on p_T one obtains the famous Gluckstern formula for N equidistant measurements with a precision σ_{mess}:

$$\boxed{\left(\frac{\sigma_{p_T}}{p_T}\right)_{\mathrm{mess}} = \frac{p_T}{0.3|z|}\frac{\sigma_{\mathrm{mess}}}{L^2 B}\sqrt{\frac{720}{N+4}}}$$

$$[p_T] = \mathrm{GeV/c},\ [L] = \mathrm{m},\ [B] = \mathrm{T}$$

Major dependencies:

- relative resolution is directly proportional to p_T
- directly proportional to the detector resolution σ_{mess} (→ aim for high resolution)
- $1 / L^2$ → measurement volume enters quadratically
- ~1 /B: gain linearly with higher magnetic fields
- ~$1/\sqrt{N}$: gain with number of measurements, however, only with square root

The influence of Coulomb Multiple Scattering:

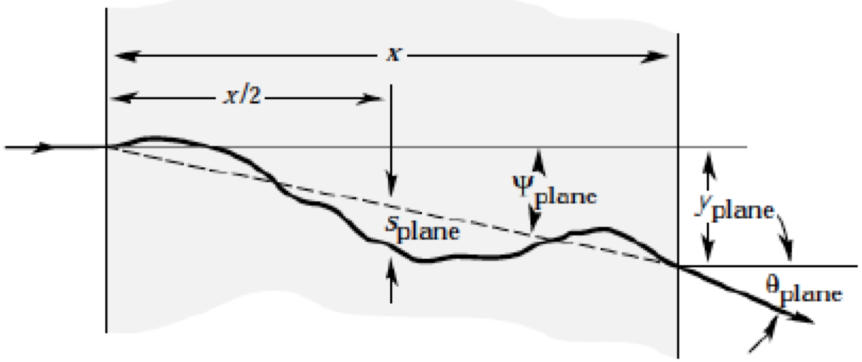

charged particles undergo multiple Coulomb scattering processes when passing through matter

average deviation in a thickness x is:

$$\langle s_{plan} \rangle = \frac{1}{4\sqrt{3}} x\,\theta_0 \;\approx \sigma_{sagitta}$$

- The scattering angle has a distribution that is almost gaussian
- At large angles deviations from gaussian distributions appear that manifest as a long tail going as $\sin^{-4}\theta/2$ (Moliere theory).
- In "thick" detectors the distribution of the lateral displacement y_{plane} should also be considered.

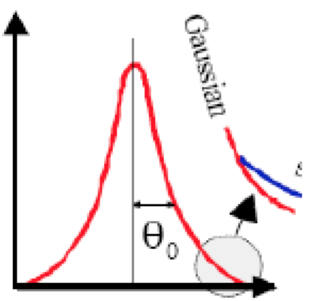

$$\frac{1}{\sin^4 \frac{\theta_p}{2}}$$

radiation length

$$\boxed{\theta_0 = \frac{13.6\,\mathrm{MeV/c}}{p\beta} z \sqrt{\frac{x}{X_0}} \left(1 + 0.038 \ln \frac{x}{X_0}\right)}$$

$$\boxed{\sigma_\kappa = \frac{8}{L^2}\sigma_s} = \frac{8}{L^2}\frac{1}{4\sqrt{3}} x\,\theta_0 \overset{x \approx L}{=} \sqrt{\frac{4}{3}}\frac{\theta_0}{L} = \boxed{\frac{0.0136\,\mathrm{GeV/c}}{p\,\beta\,L} z \sqrt{\frac{L/\sin\theta}{X_0}} (\underbrace{\sqrt{1.33}}_{N=3} - \underbrace{\sqrt{1.43}}_{N>10})}$$

Total momentum resolution:

$$\sigma_{p_T} = \frac{p_T^2}{|q|\,B}\sigma_\kappa = \frac{p_T^2}{0.3\,|z|\,B}\sigma_\kappa \quad \Rightarrow$$

in GeV/c, Tesla units

0.0136 * √1.43 / 0.3 = 0.054

$$\left(\frac{\sigma_{p_T}}{p_T}\right)_{\text{MS}} = \frac{0.054}{L\,B\,\beta}\sqrt{\frac{L/\sin\theta}{X_0}}$$

$$\left(\frac{\sigma_{p_T}}{p_T}\right)_{\text{mess}} = \frac{p_T}{0.3|z|}\frac{\sigma_{\text{mess}}}{L^2 B}\sqrt{\frac{720}{N+4}}$$

for N>10

$$[p_T] = \mathrm{GeV/c},\ [L] = \mathrm{m},\ [B] = \mathrm{T}$$

$$\boxed{\frac{\sigma_{p_T}}{p_T} = \sqrt{\left(\frac{\sigma_{p_T}}{p_T}\right)^2_{\text{mess}} + \left(\frac{\sigma_{p_T}}{p_T}\right)^2_{\text{MS}}}}$$

example: OPAL

L = 1.6 m, B = 0.435 T, N = 159, σ_{mess} = 135 µm

$$\frac{\sigma_{p_T}}{p_T} = \sqrt{(0.0015\,p_T)^2 + (0.02)^2}$$

p_T in GeV

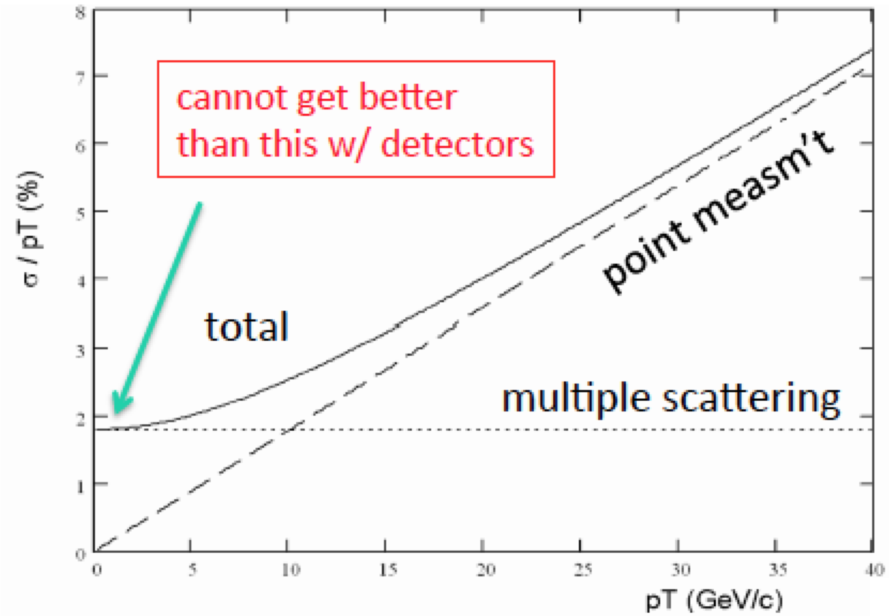

5.2 Magnetic Spectrometers

Nearly all particle physics experiments at accelerators have a magnetic spectrometer to measure the momentum of charged particles

Commonly used magnets: **Solenoids, Dipoles and Toroids**

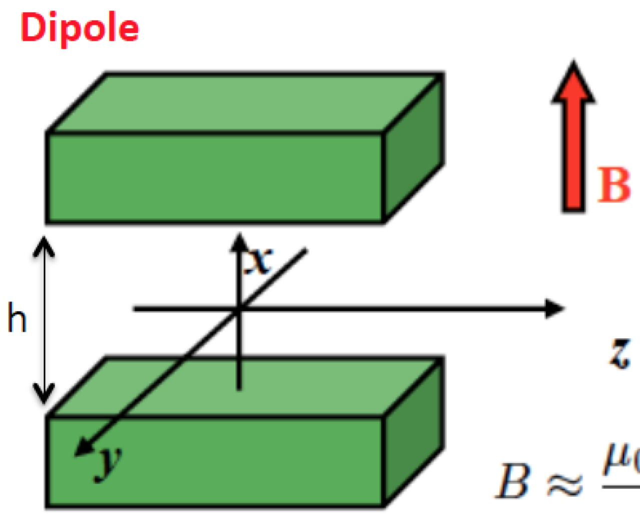

$$B \approx \frac{\mu_0 N I}{h}$$

- **rectangular symmetry**
  - deflection in y - z plane
  - tracking detectors are arranged in parallel planes along z
  - measurement of curved trajectories in y - z planes at fixed z

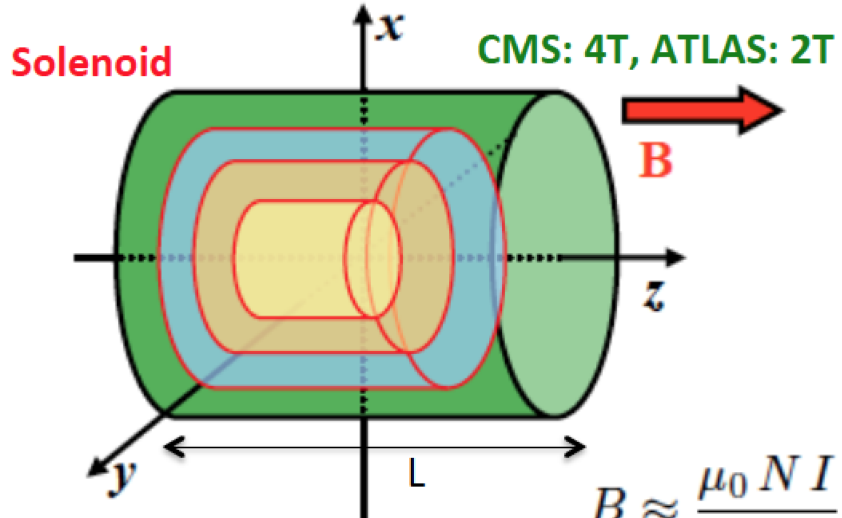

$$B \approx \frac{\mu_0 N I}{L}$$

- **cylindrical symmetry**
  - deflection in $x - y$ (r - ϕ) plane
  - tracking detectors are arranged in cylindrical shells along r
  - measurement of curved trajectories in r-ϕ planes at fixed r

Toroid

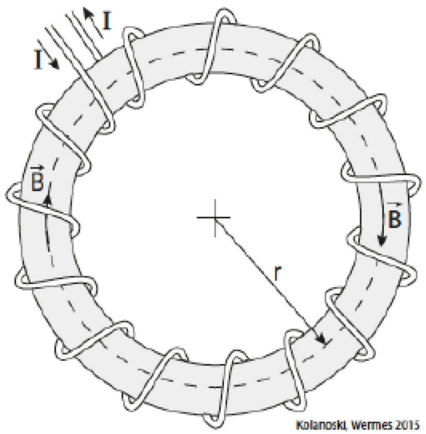

(a)

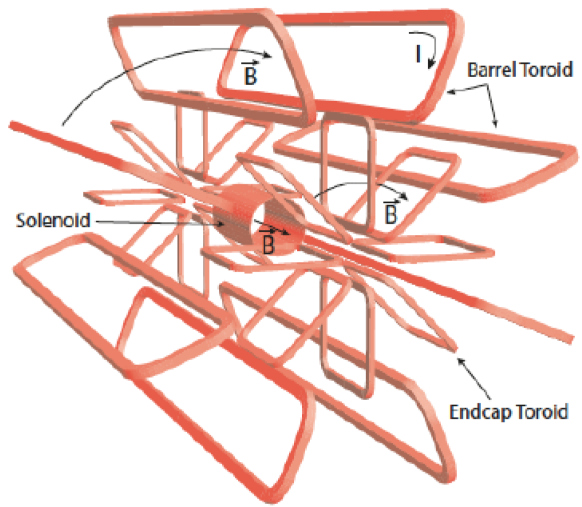

(b)

- **azimuthal symmetry**
  - deflection in (r - z) - plane
  - tracking detectors are (in ATLAS) also arranged in cylindrical shells
  - but measurement of curved trajectories in r-z planes at fixed r

ATLAS: 0.5 T

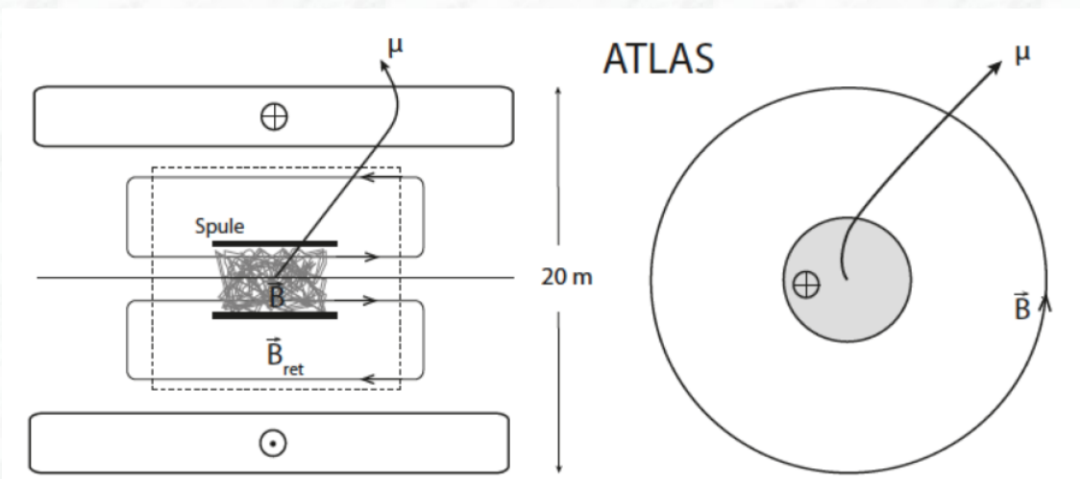

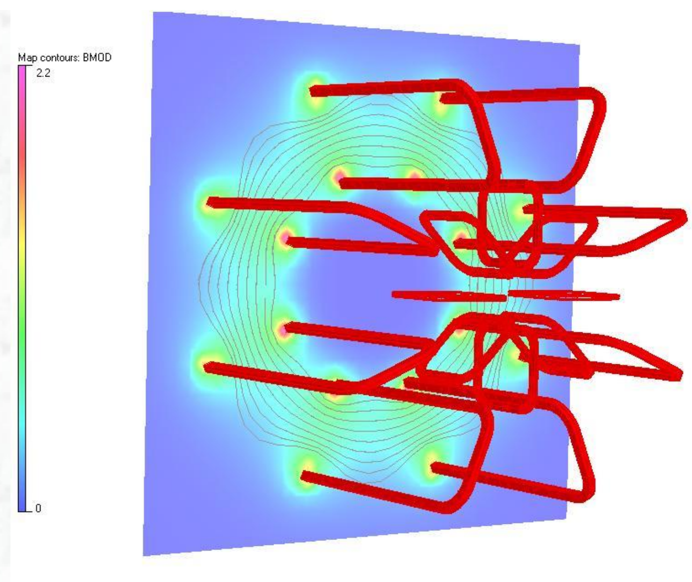

Tracking in LHCb: Dipole field (forward region, fixed target)

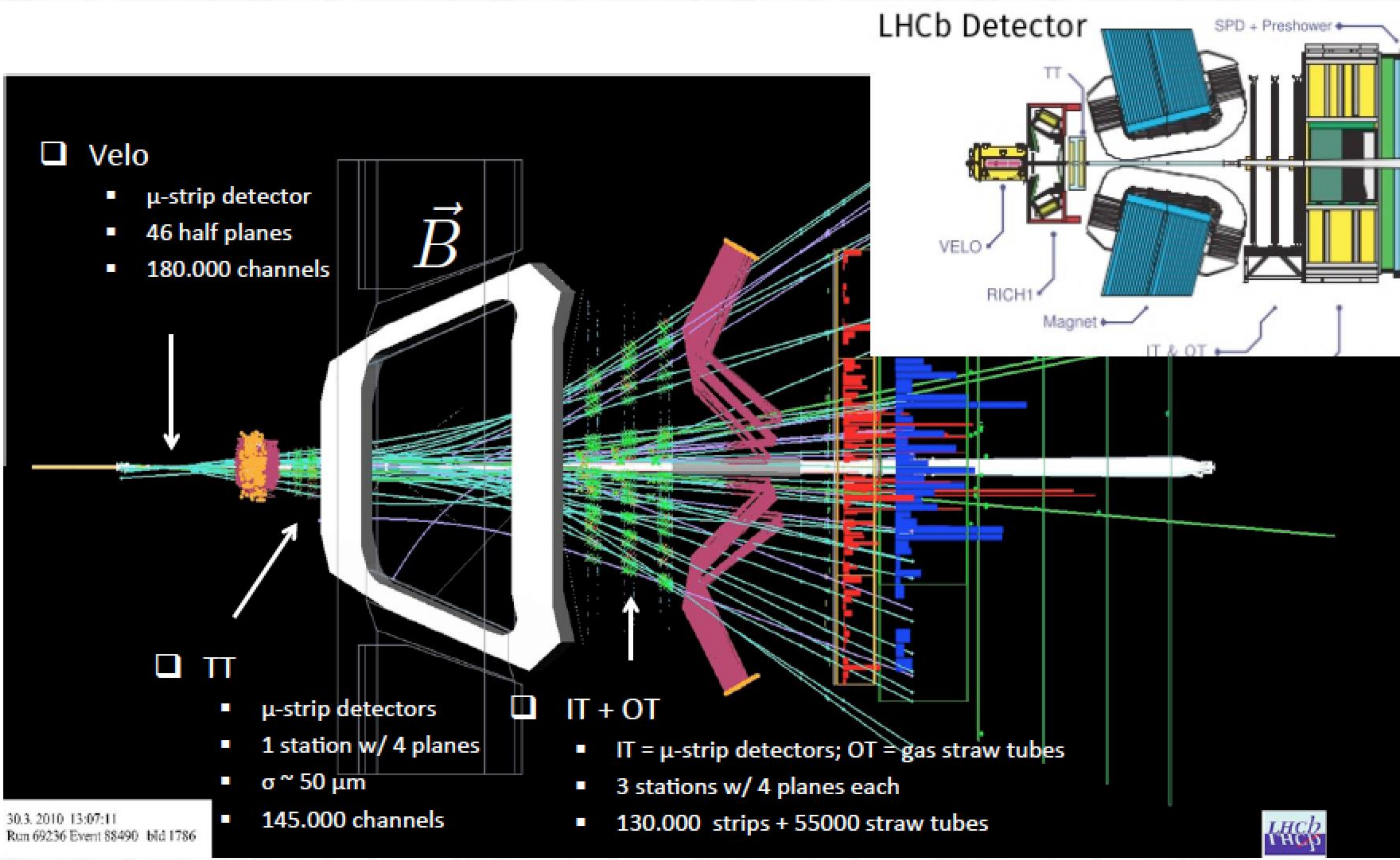

Tracking in LHCb: Dipole field   (forward region, fixed target)

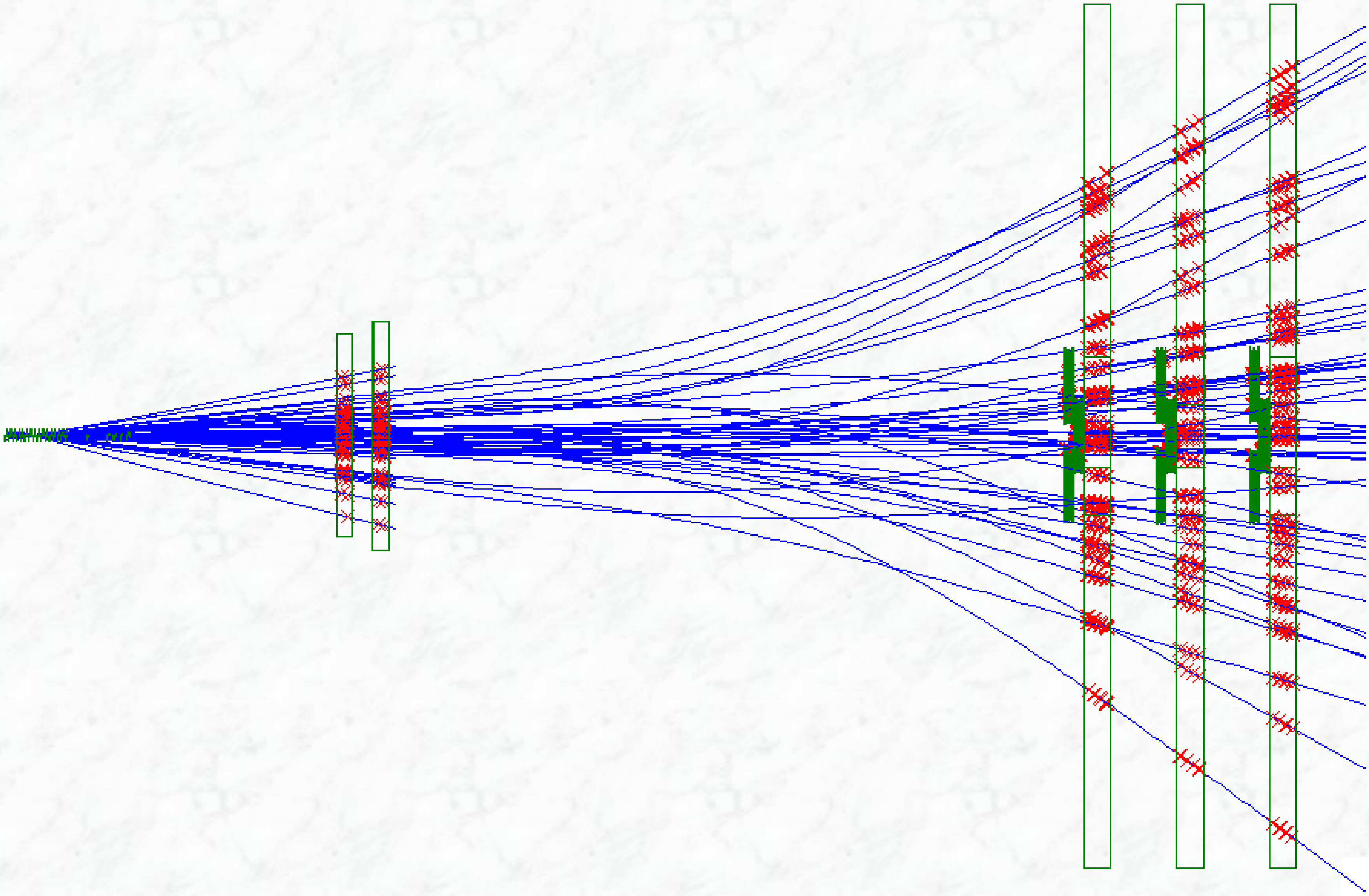

Tracking in CMS: Solenoid field

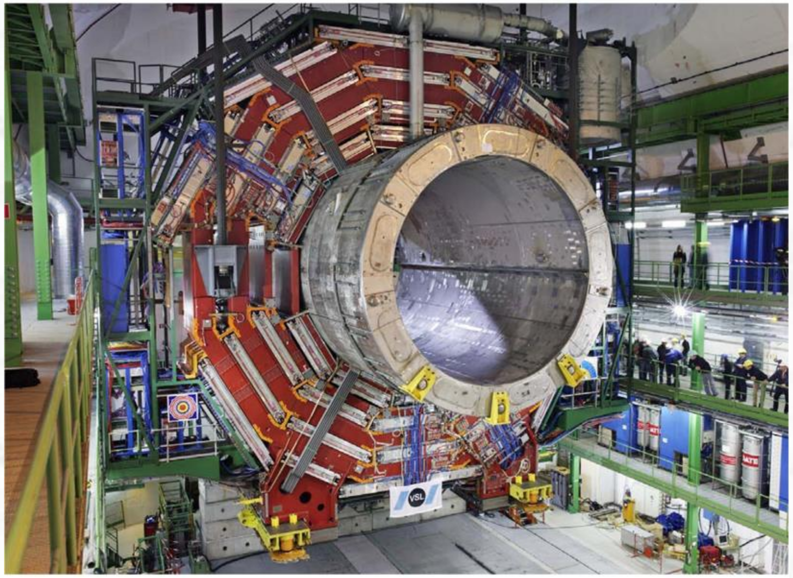

Magnetic field of 3.8 Tesla

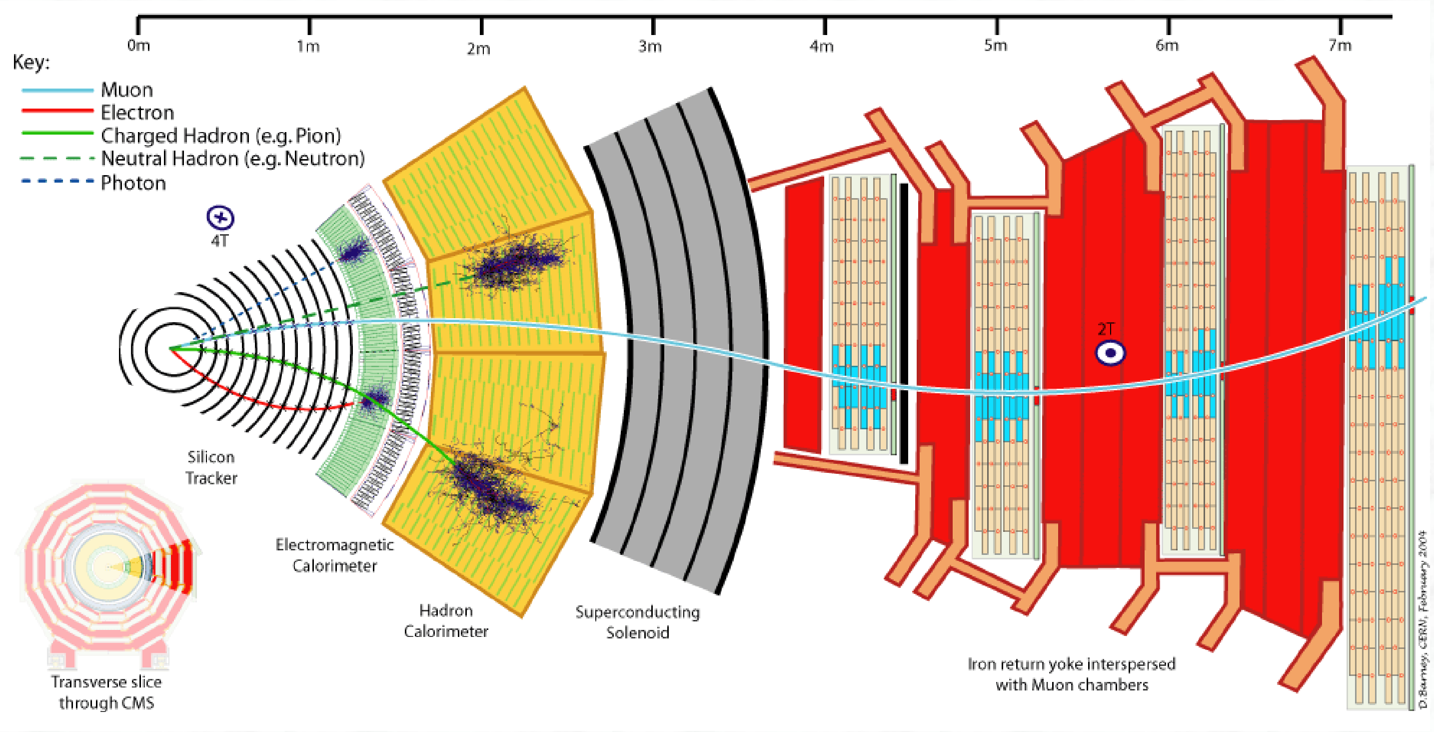

Muons in ATLAS: Toroidal field

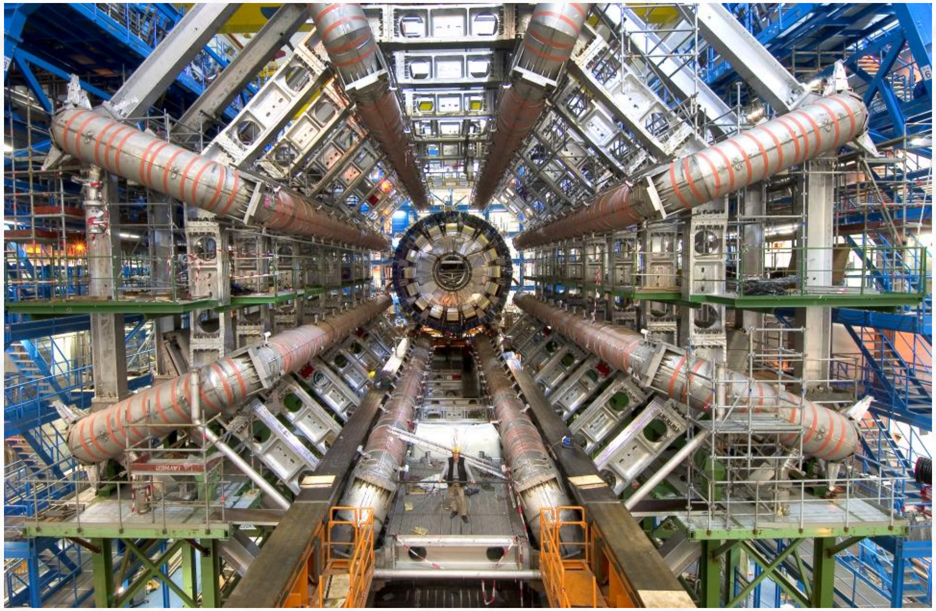

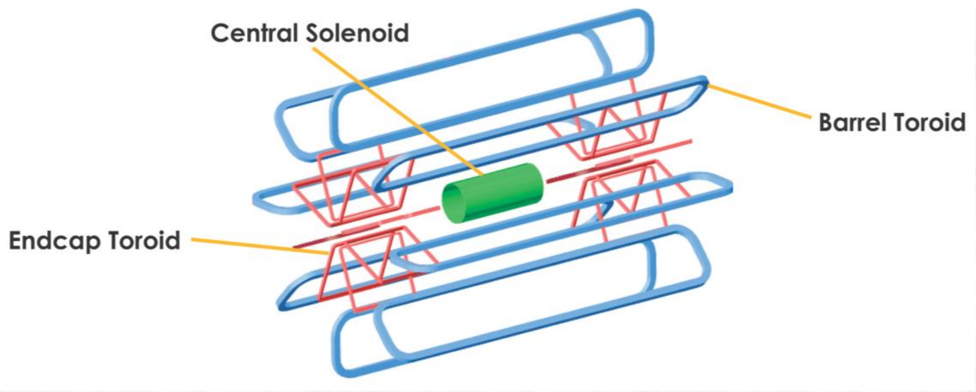

5.3 Multi-wire proportional chamber

- In order to extract space / coordination information efficiently, Multi-Wire-Proportional Chambers (MWPCs) were used for long time

  G. Charpak (1968, Nobel prize,1992)

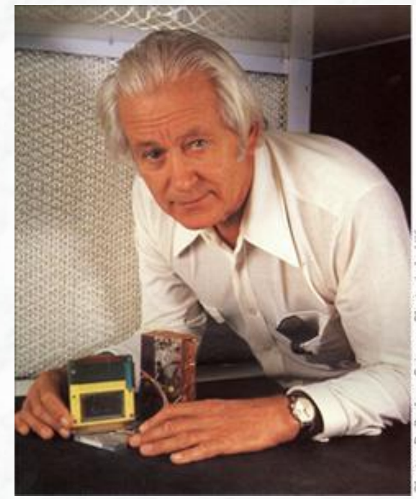

- Principle:
  - Put many anode wires in parallel, in one volume
  - High voltage: each wire acts as an independent proportional counter (gas amplification)

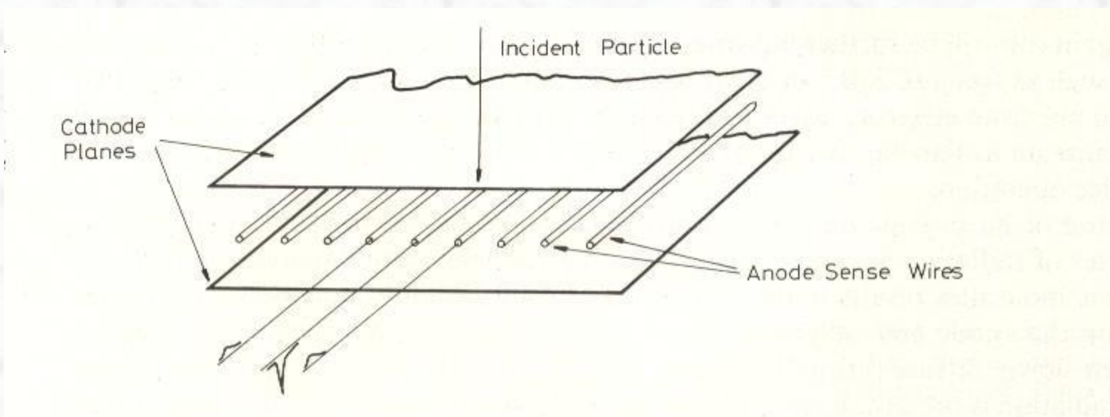

- Every wire acts as an independent proportional tube

  → every anode wire is read out separately → space information

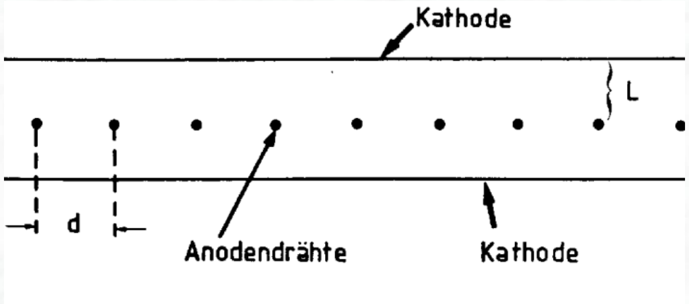

- Typical parameters: distance between wires: d = 2 mm
  distance anode-cathode: L = 7-8 mm
  diameter of anode wires: 10 – 30 μm
  (thin wire → high electric field → gas amplification)

- Achievable coordinate resolution: $\sigma = d / \sqrt{12} \sim 600\ \mu m$

This resolution is not adequate for today's LHC experiments;
(however, was sufficient for experiments in the 1970/80s)

Electrical field configuration:

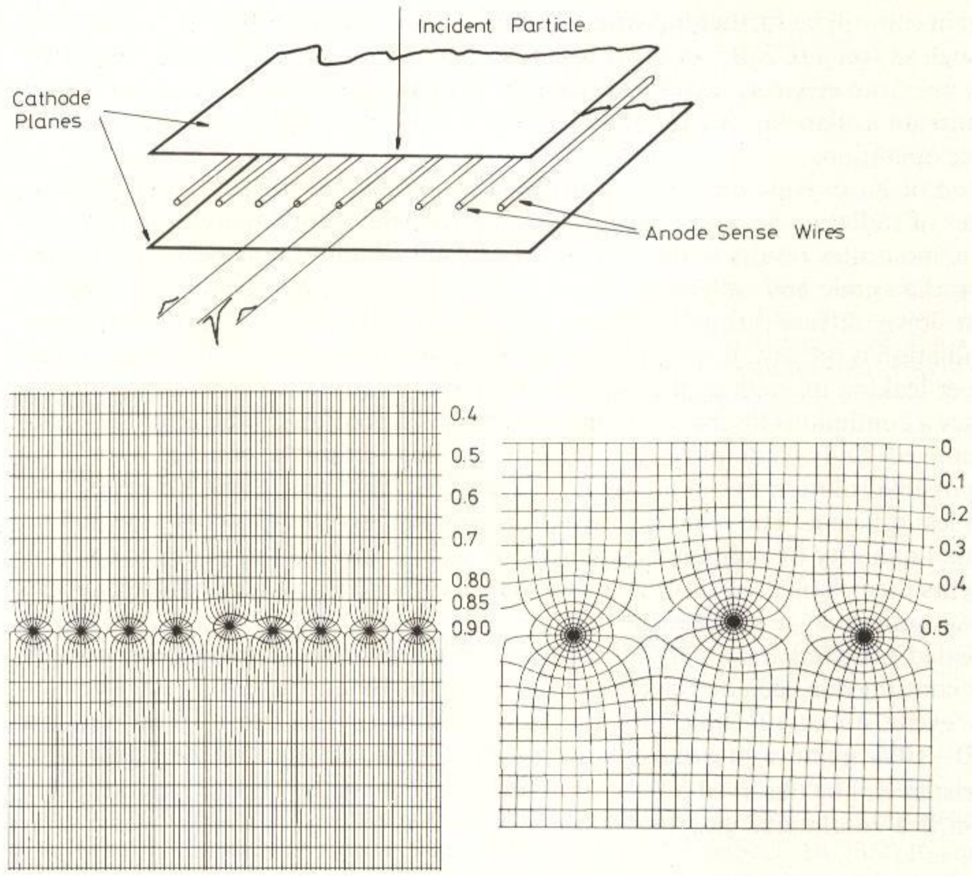

Fig. 6.8. Electric field lines and potentials in a multiwire proportional chamber. The effect of a sli
displacement on the field lines is also shown (from *Charpak* et al. [6.16])

- Homogeneous field, except in the vicinity of the the anode wire
- Lines of equal potential are parallel to cathode in large part of ionisation volume
- Every wire is read out individually → spatial information however, rather large number of readout channels
- Electrons drift to next anode wire, positive ions drift to cathode
- The functionality of the MWPC can be significantly increased if induced signals on cathode are also read out → second coordinate

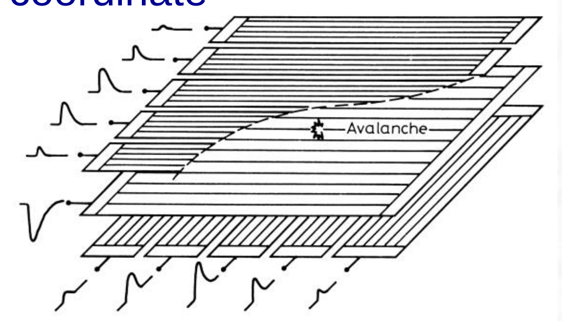

Principle of gas amplification and ion drift:

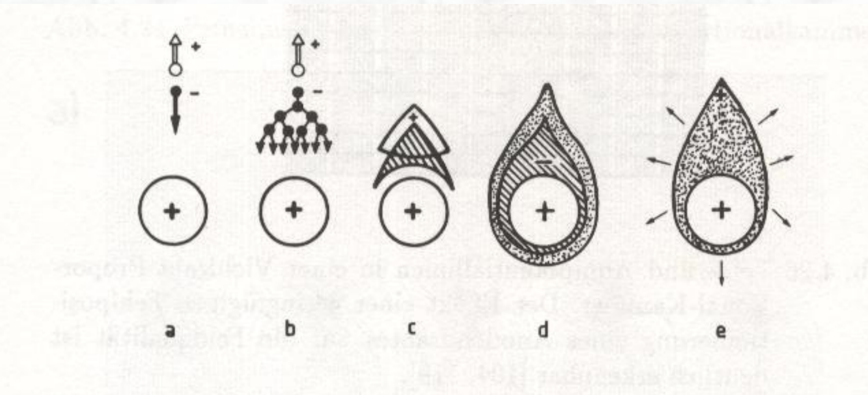

- 1/r E-field in region of anode wire
  → gas amplification (A ~10^5)

- Typical gas mixtures used:
  - Ar + CH_4,
  - Ar + CO_2,
  - Ar + isobutane, ..

- Electrons drift to next anode wire

- Positive ions drift to cathode

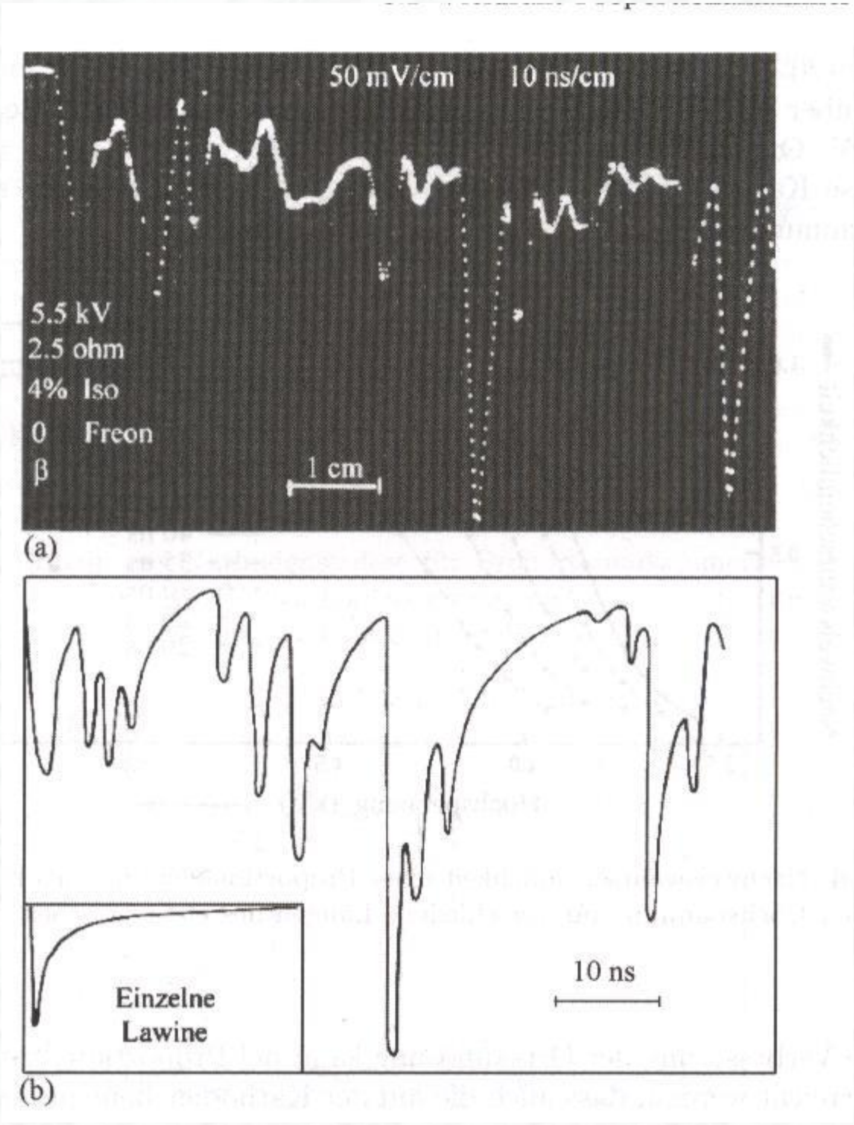

Time structure of the anode signal of a MWPC, recorded with a short electronics response / shaping time (τ < 10 ns) [from Ref. 3]

→ very fast rise time of individual avalanches

- Possibilities for second coordinate measurement:

(i) Crossed chambers (90°), chamber positions known in z-direction

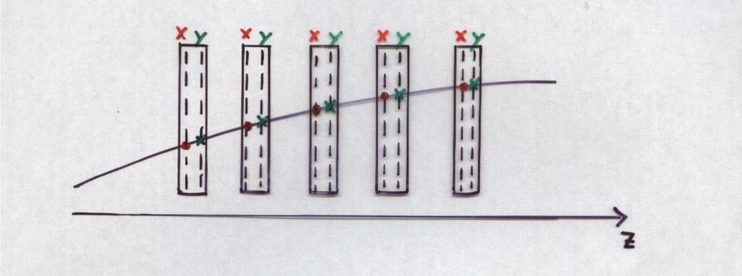

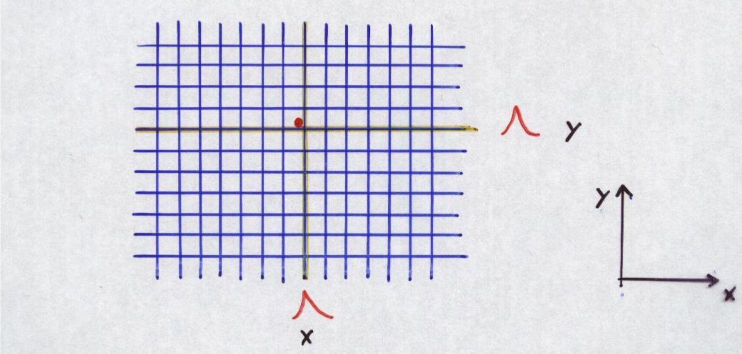

→ measurements of both coordinates at fixed z-positions (x,z_1) and (y,z_2)

MWPC-precision (~600 μm) in each coordinate

- Possibilities for second coordinate measurement:

(i) Crossed chambers (90°), chamber positions known in z-direction

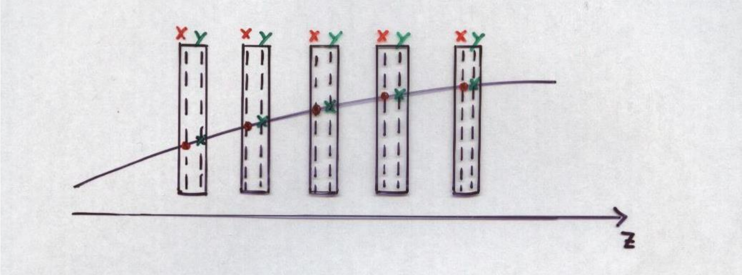

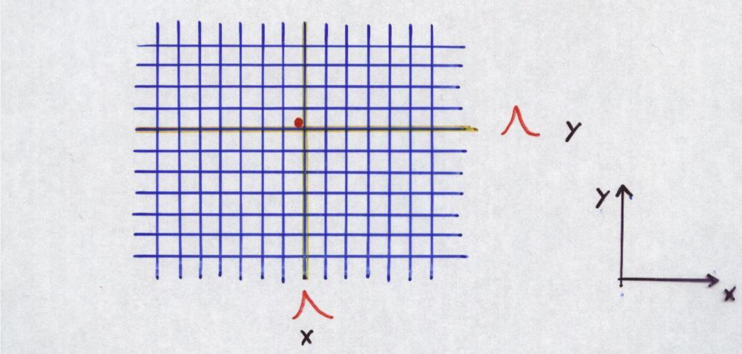

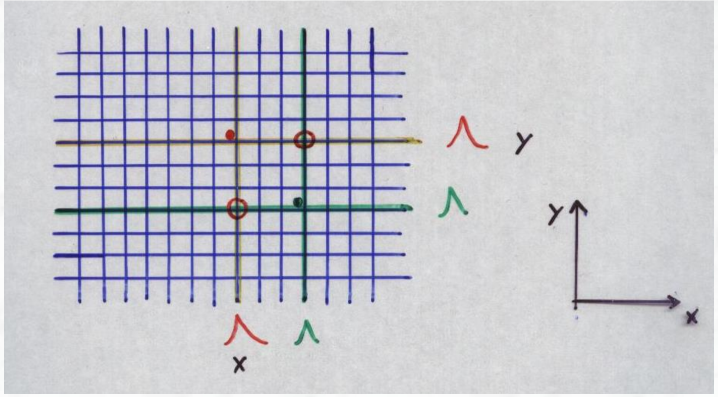

→ measurements of both coordinates at fixed z-positions (x,z_1) and (y,z_2)

MWPC-precision (~600 μm) in each coordinate

Ambiguities, for more than one particle
→ ghost points

Not well suited for high particle multiplicities

(ii) Stereo layers (small stereo angles, α = 3-5°)

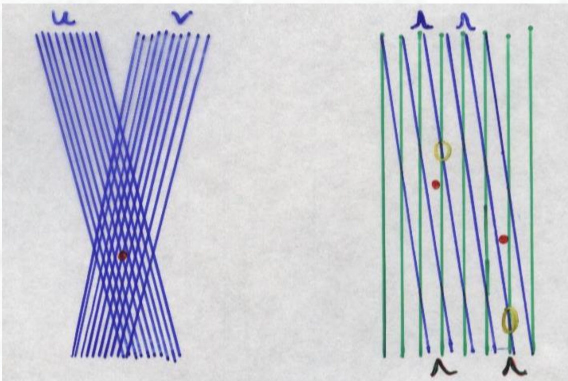

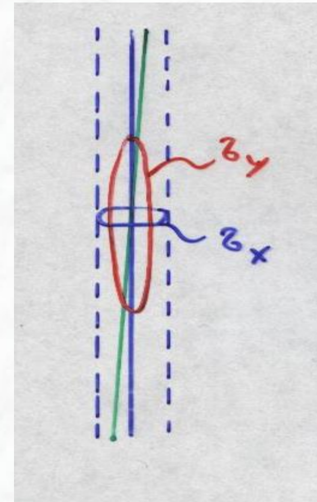

→ Reduced ambiguity problem due to smaller overlap

often so-called triplet layers are used (-3°, 0°, +3°) (u, x, v) coordinates

However, degraded resolution in the second coordinate

0° layers: → σ_x ~600 μm

stereo layers: → $\sigma_y \sim \sigma_x / \sin \alpha$

for stereo angle α = 3-5°
→ σ_y ~ O(cm)

(iii) Cathode strip readout (segmented cathode)

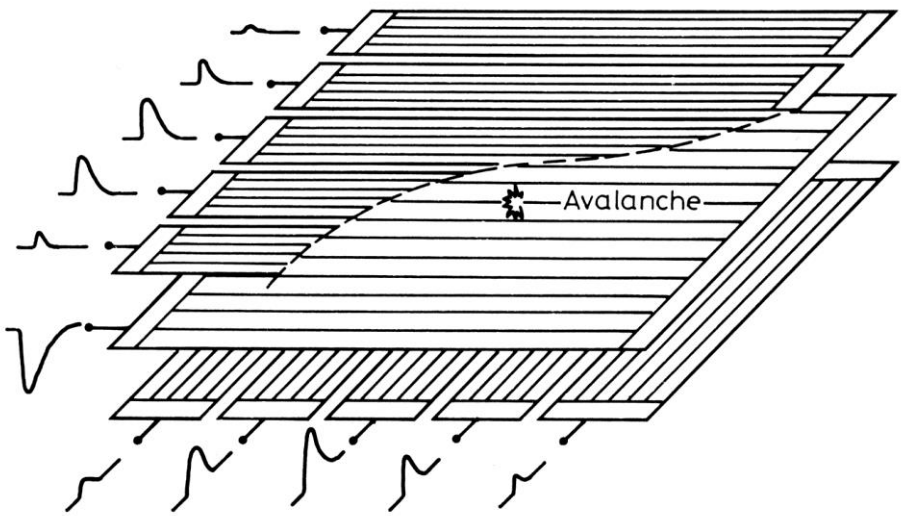

→ Improvement of the coordinate resolution by calculating centre-of-gravity (weighted by charge = pulse height) of the cathode signals

$y = \Sigma (Q_i \; y_i) \; / \; \Sigma Q_i$ where: Q_i = Charge on cathode strip i
y_i = strip position

→ achievable resolution: 50 – 100 μm !

(iv) Charge division (on anode wire)

Readout the anode wire (resistive wire) at both ends (two amplifiers) and use the fact that the resistivity is proportional to the wire length

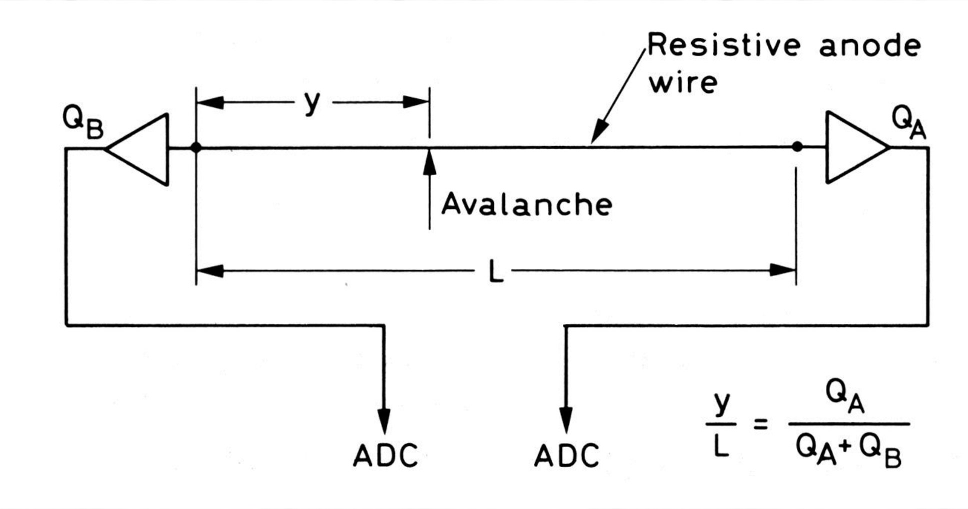

→ $y = L \quad Q_A / (Q_A + Q_B)$ where: L = wire length

→ Typical resolutions achieved: ~1% of the wire length

$\mathcal{O}$(cm)

5.4 Drift chambers

- Measure not only the pulse height, but also the time when a signal appears with respect to an external trigger signal

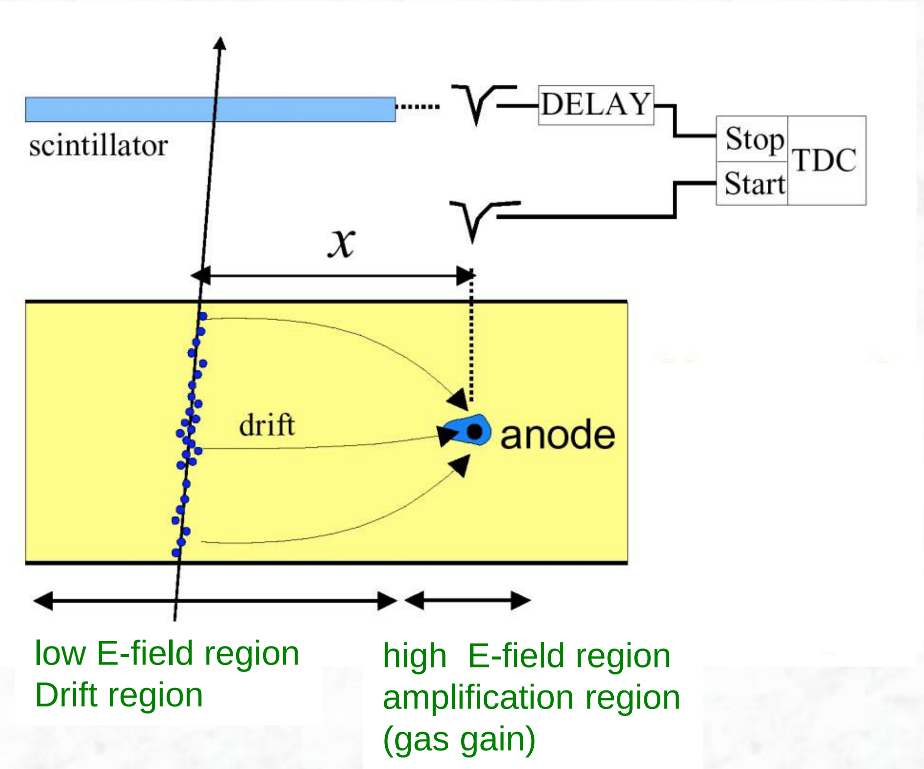

- Get external time reference t_0
  (fast scintillator or beam timing)

- Measure arrival time t_1 of electrons at the anode

- Coordinate reconstruction:

$$x = \int_{t_0}^{t_1} v_D(t)\, dt$$

Requires a precise knowledge of the drift velocity $v_D(t)$
typical drift velocity: v_D = 5 cm / μs

(as function of the position in the detector, or space-drift time relation)

- Drift chambers have, like MWPC, a left-right ambiguity

Main advantages of a drift chamber:

- Position perpendicular to the anode wire can be extracted from a space-drift-time relation
  (has to be known, it is linear, if the drift velocity is constant over the drift volume)

  However, it requires an additional time measurement (TDC)

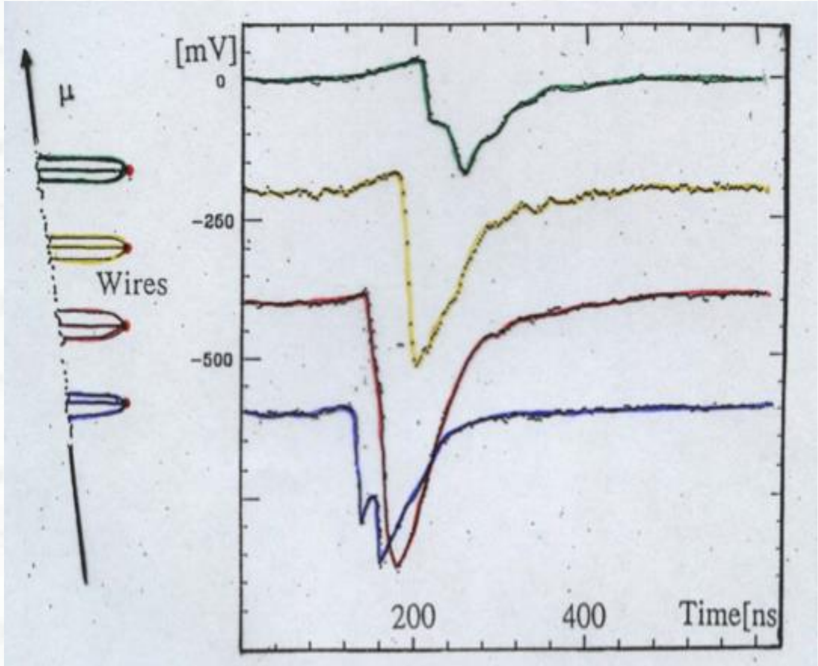

Measured signals in a drift chamber (clear space-time dependence visible, fluctuations in pulse form)

- Typical drift distances: 5 – 15 cm
  → more economical, less readout channels,
  a much larger sensitive volume can be covered per readout channel

- Improved coordinate resolution, typical values: **$\sigma \sim$ 50 – 200 μm**

  It is limited by diffusion of the drifting electron clouds, electronics (time measurements)

- However, challenging mechanics for large surface drift chambers (> 2 x 2 m^2)
  electrostatic repulsion of wires → oscillations
  sagging of wires (due to gravitation) → field inhomogeneities, affect spatial precision
  → wires have to be strained (large chambers, several thousand wires, tension can reach a few tons on end plates)

Electric field formation:

- So-called field forming wires are introduced to avoid low-field regions, i.e. long drift times

- Introduce additional wires on negative potential between anode wires

  (cathode on ground, anode on positive potential)

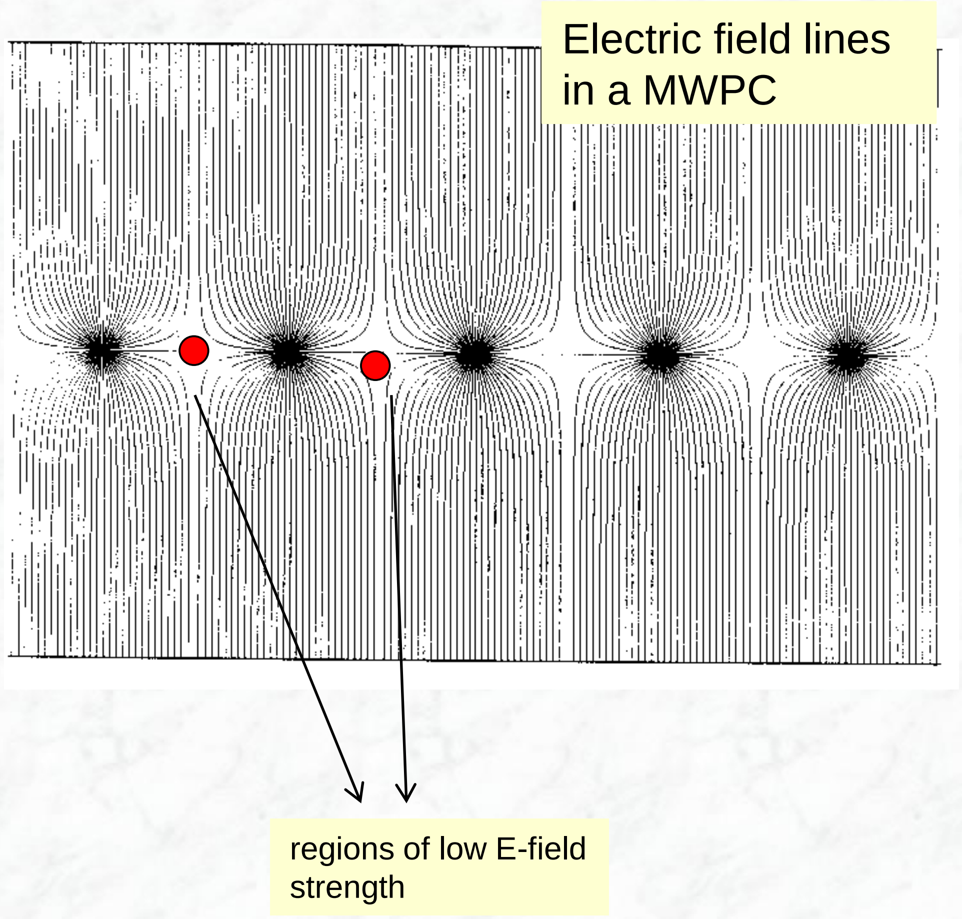

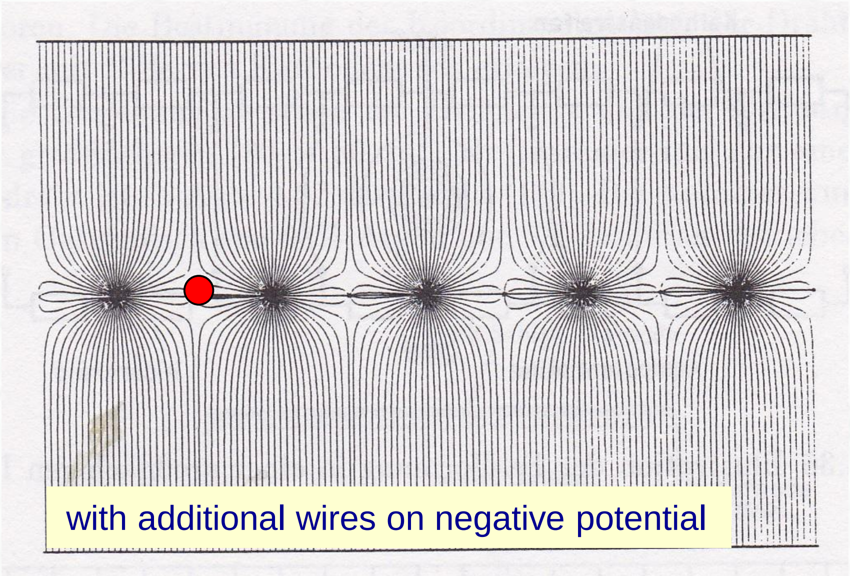

Electric field formation:

- Drift cells can be defined by putting negative potential at cell boundaries, and using voltage divider chains to define a graded potential on cathode strips

  → well defined equipotential lines, uniform field gradient

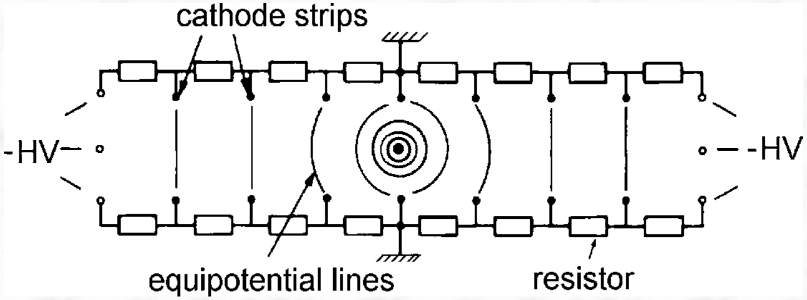

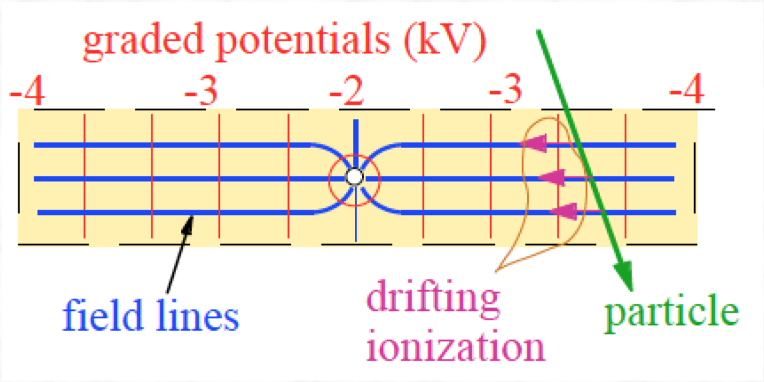

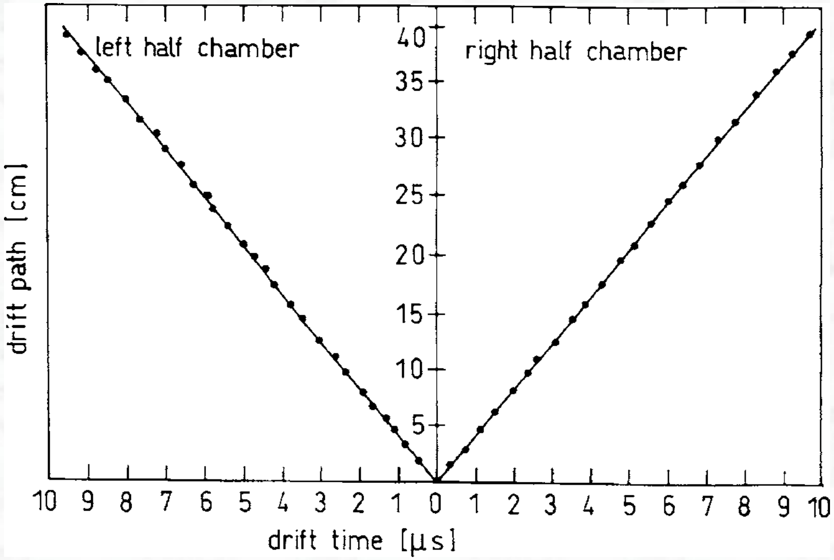

Space-drift-time relation for a large drift chamber (80 cm x 80 cm) with only one anode wire (from Ref. [3])

Contribution to the spatial resolution:

1. Time resolution of the electronics

   $\sigma_t \sim 1$ ns, $v_D = 5$ cm / μs $\rightarrow$ $\sigma_x = v_D\, \sigma_t = 50\ \mu$m

2. Diffusion of drifting electrons
   (dominant for large drift distances)

3. Statistical fluctuations in the primary ionization and differences in drift paths
   (important for small distances to the anode wire)

4. Mechanical tolerances
   (accuracy of the wire position, sagging, etc…, depends on the chamber dimensions)

5. Inhomogeneities on the electrical field strength

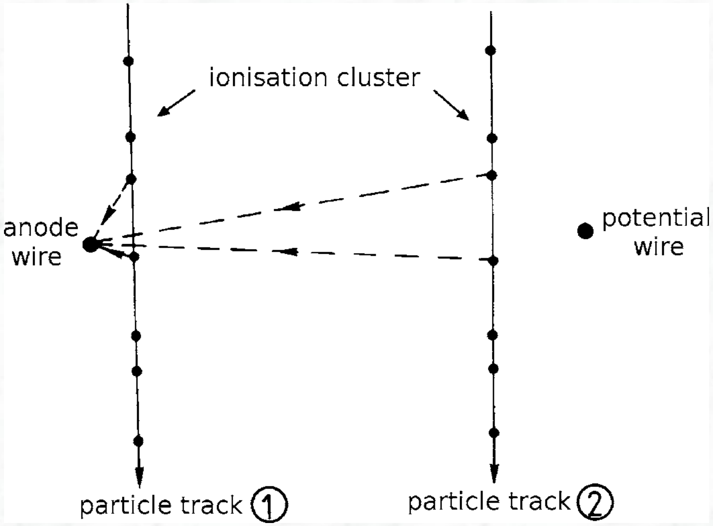

Total spatial resolution:

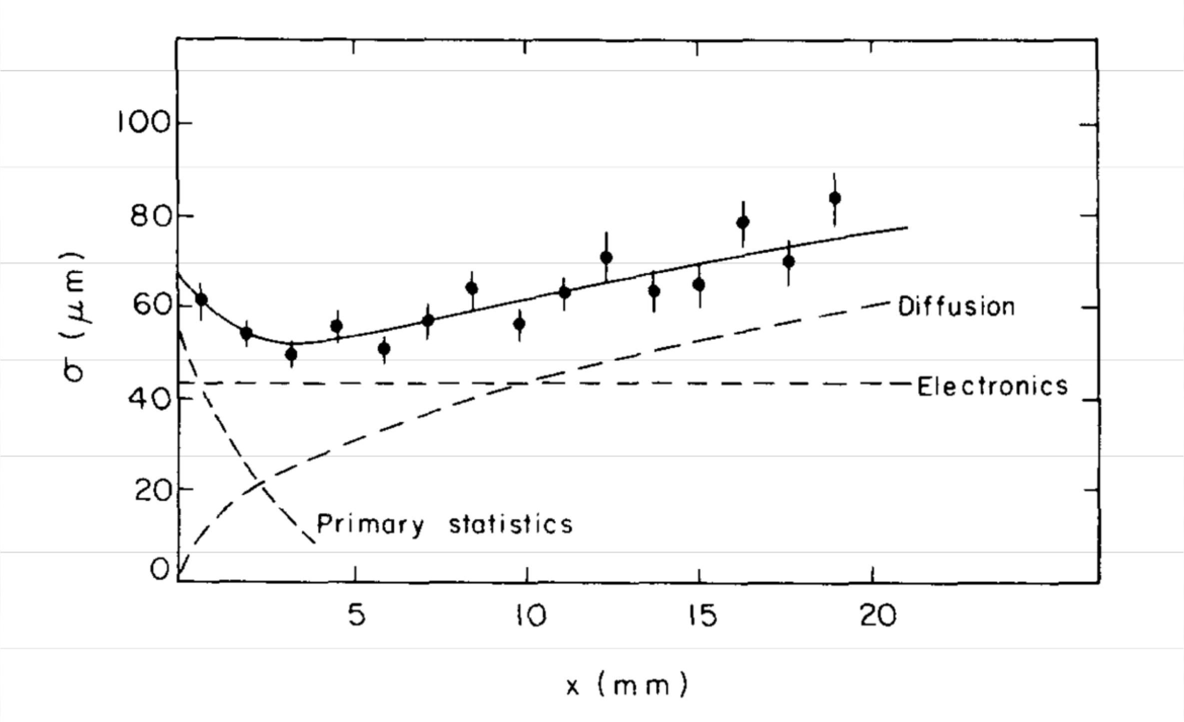

Example of the spatial resolution achieved in a small drift chamber (80 cm wires) and the decomposition into the various components (from Ref. [3])

- Diffusion is dominant for large drift distances
- Fluctuations in path length and primary ionization statistics dominate the resolution for short drift distances

Reconstruction of the second coordinate:
(along the wire, i.e. z-coordinate in cylindrical drift chambers)

- Charge division
- Small angle stereo layers
- Cathode strips work only for planar chambers

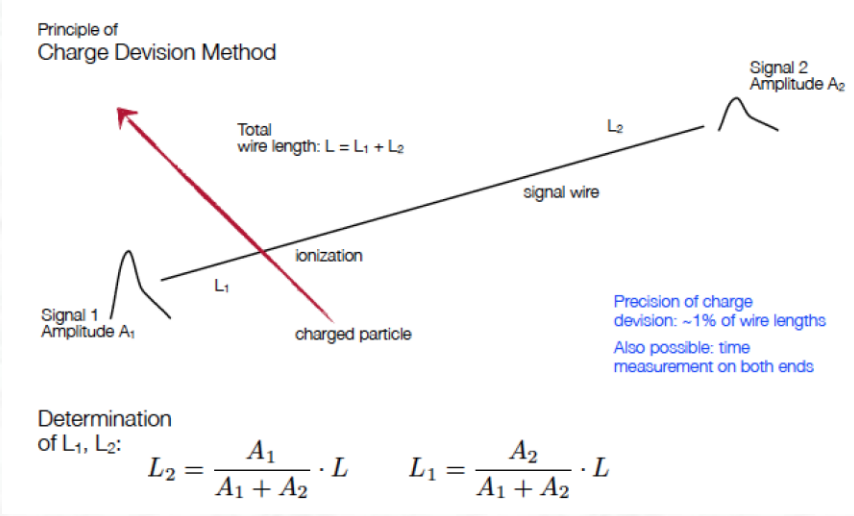

Resolution of the left-right ambiguity:

- Staggered layers in planar chambers, shift by half a drift cell

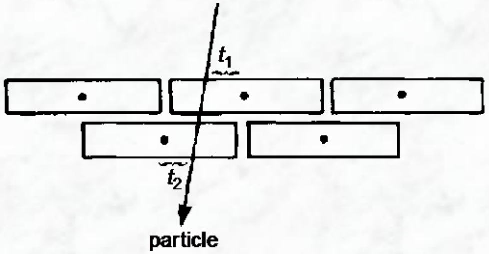

- Jet-chamber geometry, staggered anode wires (red) in cylindrical geometries

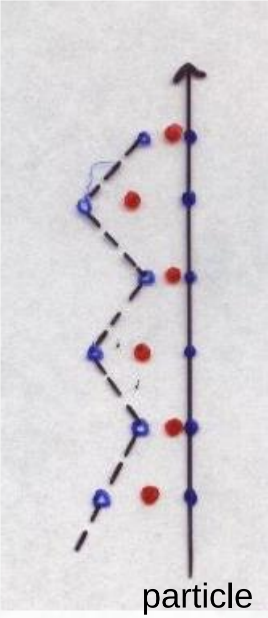

Corrections for the Lorentz-angle:

In general the E and B-fields are perpendicular in cylindrical drift chambers

→ Lorentz angle,
Drift velocity has a component in E x B-direction

Reminder:

$$\vec{v}_D = \frac{\mu|\vec{E}|}{1+\omega^2\tau^2}\left[\hat{\vec{E}} + \overbrace{\omega\tau\hat{\vec{E}}\times\hat{\vec{B}}}^{\substack{\text{Component}\\ \perp \text{ to E,B}}} + \overbrace{\omega^2\tau^2(\hat{\vec{E}}\cdot\hat{\vec{B}})\hat{\vec{B}}}^{\substack{\text{Component}\\ \text{in direction of B}}}\right]$$

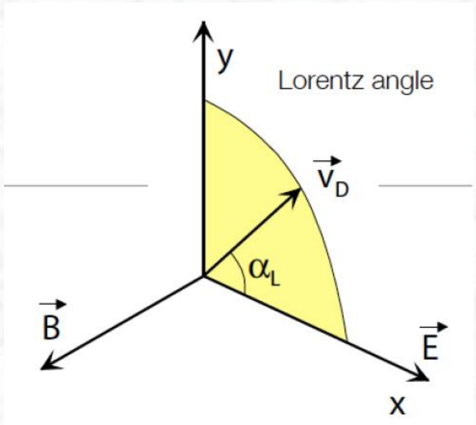

→ space-drift-time relation affected, has to be taken into account

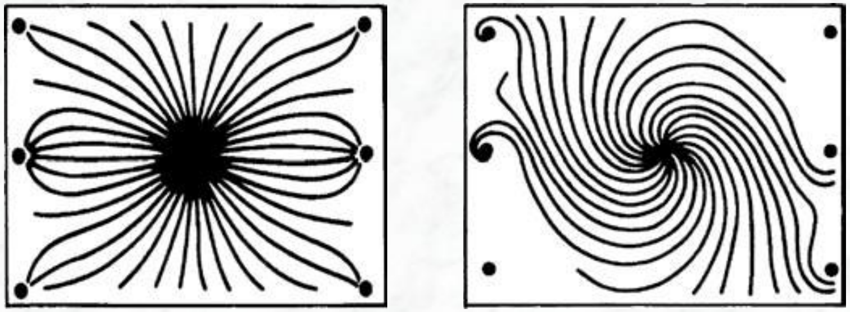

Drift trajectories of electrons in an open rectangular drift cell without (left) and (inside) a magnetic field B perp. to E (from Ref. [3])

Cylindrical Drift Chambers:

- Used in inner tracking volume of collider experiments in solenoidal magnetic fields
- Characteristica: cylindrical symmetry, open drift cell geometry
- Require: simple space-time relation, given the E-, B-fields and drift cell geometry

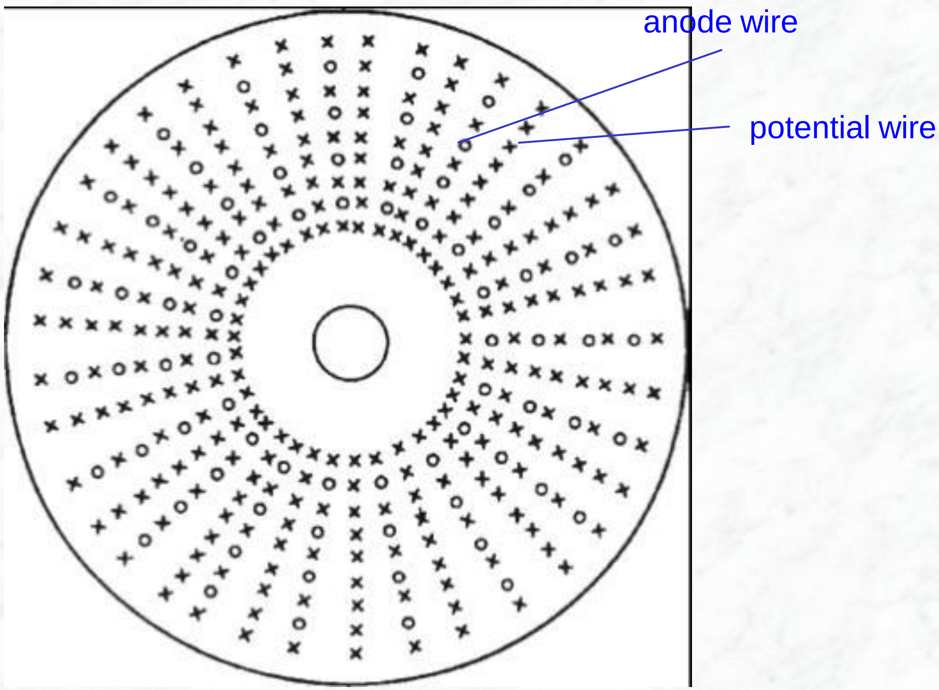

Illustration of a cylindrical drift chamber for a collider experiment (from Ref. [3])

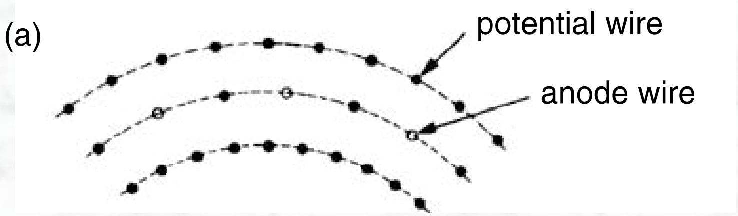

Illustration of three neighbouring drift cells (from Ref. [3])

anode wires: ~30 μm diameter
potential wires: ~100 μm diameter

Different Drift Cell Geometries for cylindrical drift chambers

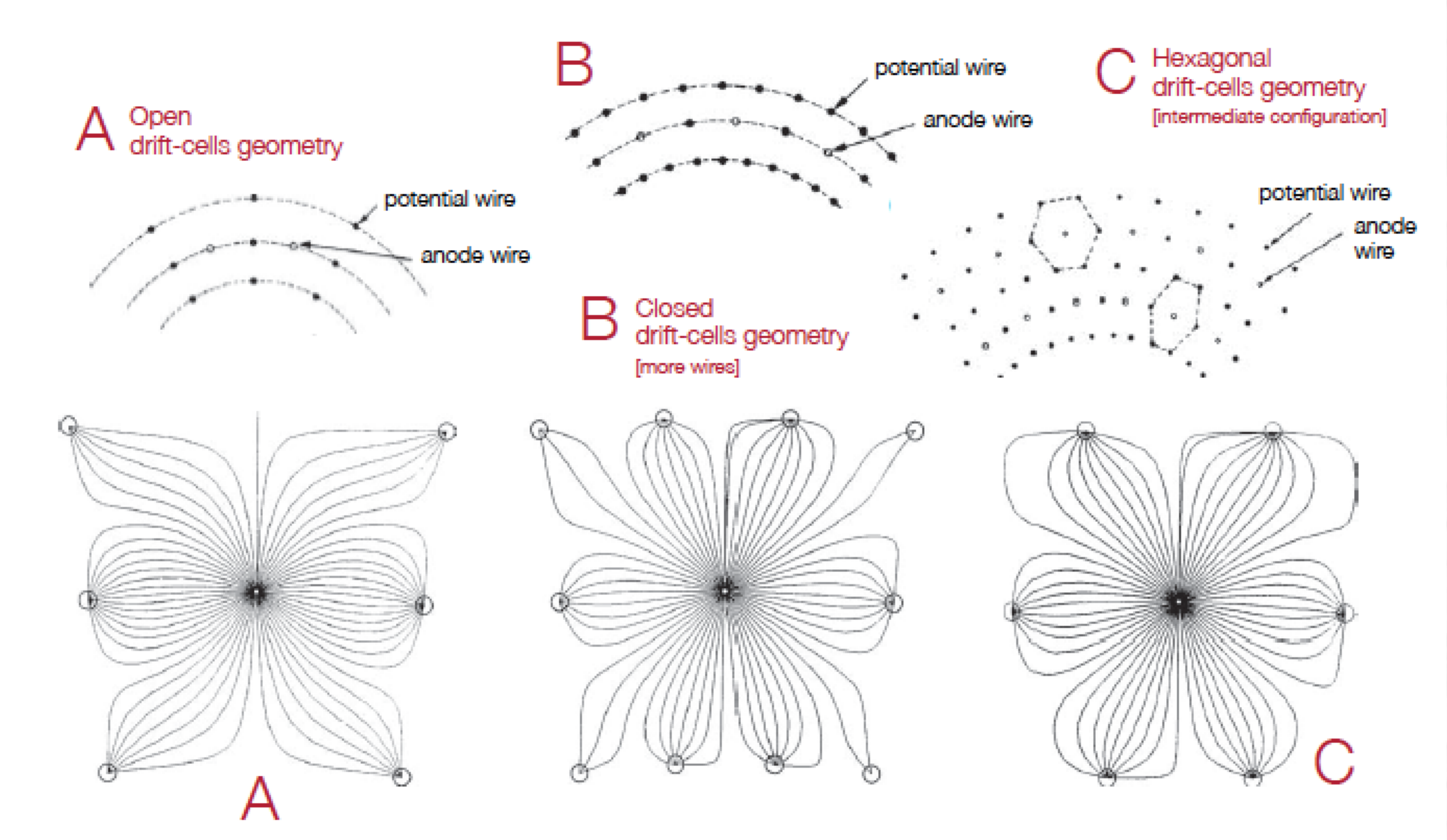

Closed geometry: better field quality, however, more wires have to be stretched;
The hexagonal structure represents a compromise solution

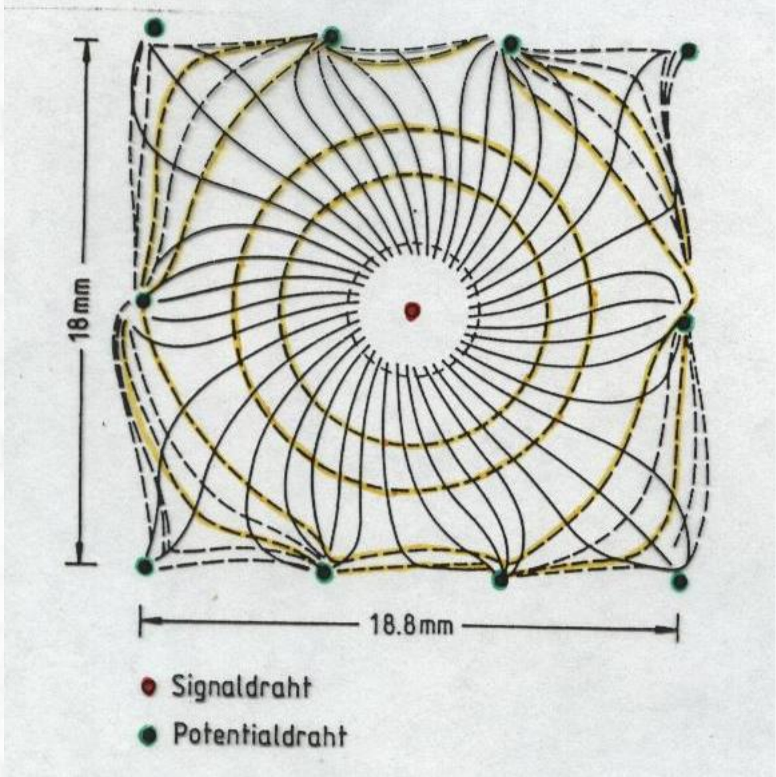

Example of a closed drift cell, as built for the drift chamber of the ARGUS experiment at DESY, Hamburg. Shown in yellow are lines with the same drift time.

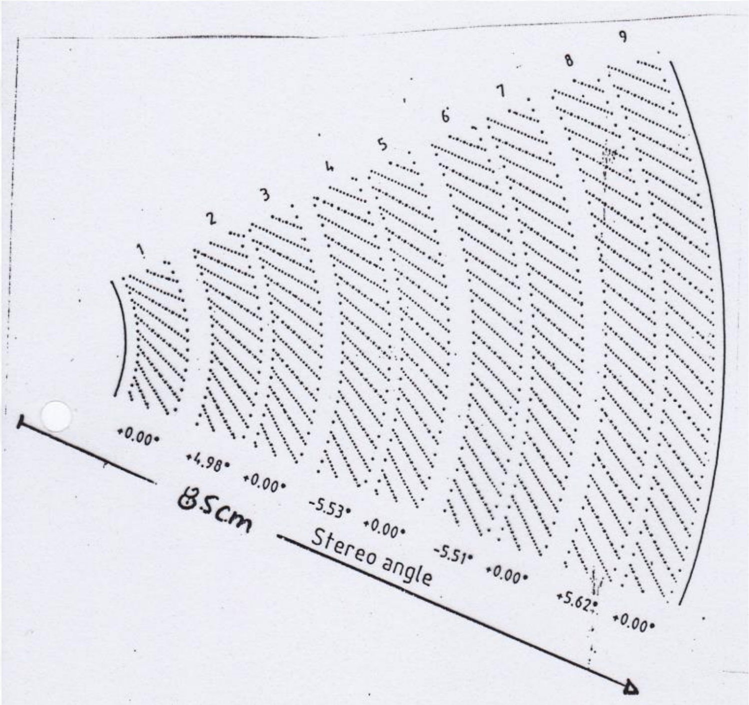

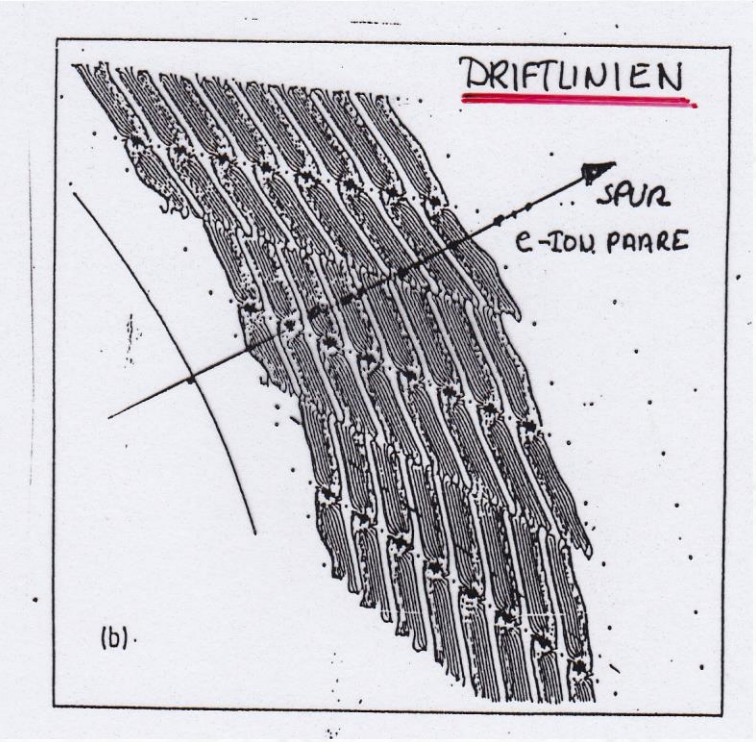

Octant of the drift chamber of the ZEUS experiment
at DESY Hamburg;

Magnetic field 1.6 Tesla

Drift cells oriented to compensate
the Lorentz angle

“Jet Chamber” geometry

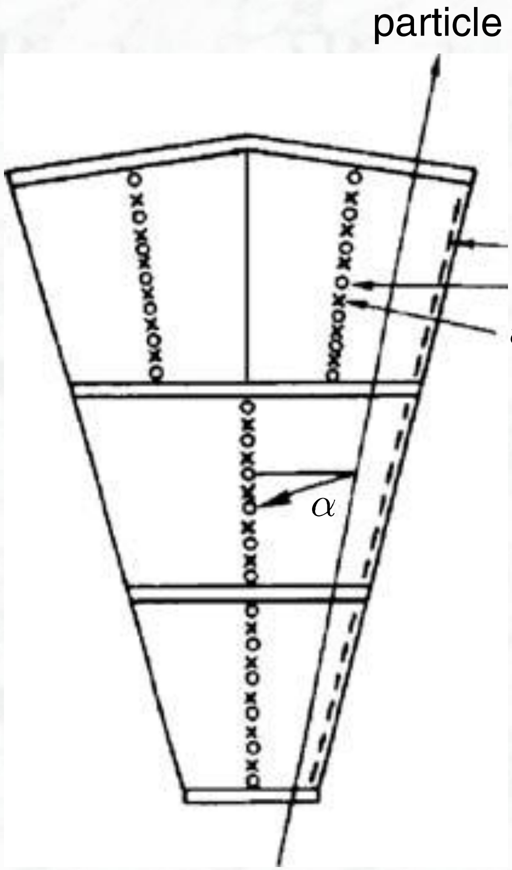

Segment of a Jet drift chamber
(from Ref. [3])

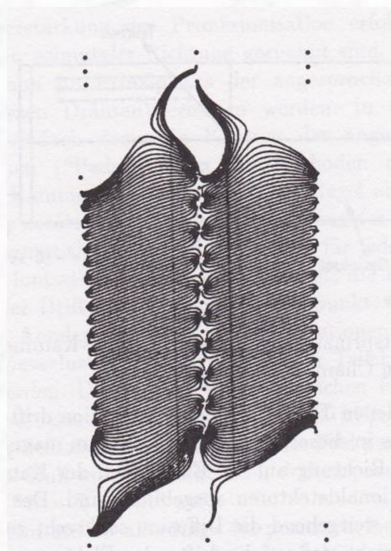

Calculated drift trajectories
in a drift cell of a jet chamber
(from Ref. [3])

Important features:

- Large number of signal wires in the centre of large trapezoidal drift cells

  → allows for good dE/dx measurement

- Large drift cells → long drift times

- Left-right ambiguities resolved by staggered anode wires

JADE: B = 0.45 T
Lorentz-angle: 18.5°

Prominent experiments with Jet Chambers: JADE at PETRA (DESY, 1980s)
OPAL at LEP (CERN, 1990s)

Jet structures seen in the JADE Jet Chamber (reaction $e^+e^- \rightarrow qqg$)

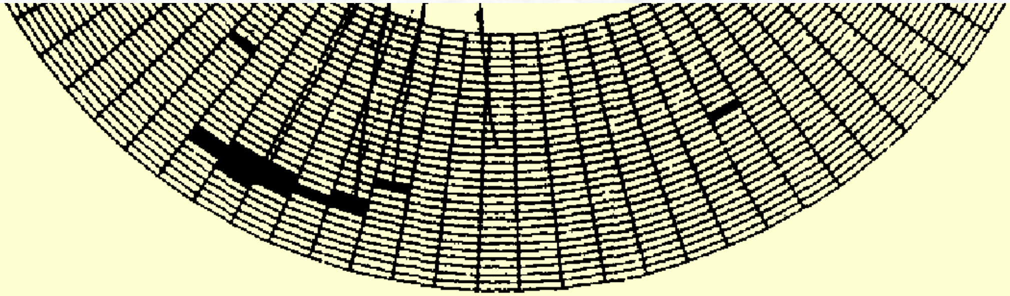

b

. a three-jet event in the JADE detector.

strongly boosted into the parton direction and th
al inspection (fig. 5.1a). The transverse momentum o
d with an average $\langle p_t \rangle \sim 300$ MeV, the same value a
shows a different structure, the events are more plana
1b). These features can be quantified for example b

(5.20

Japan-Deutschland-Engla

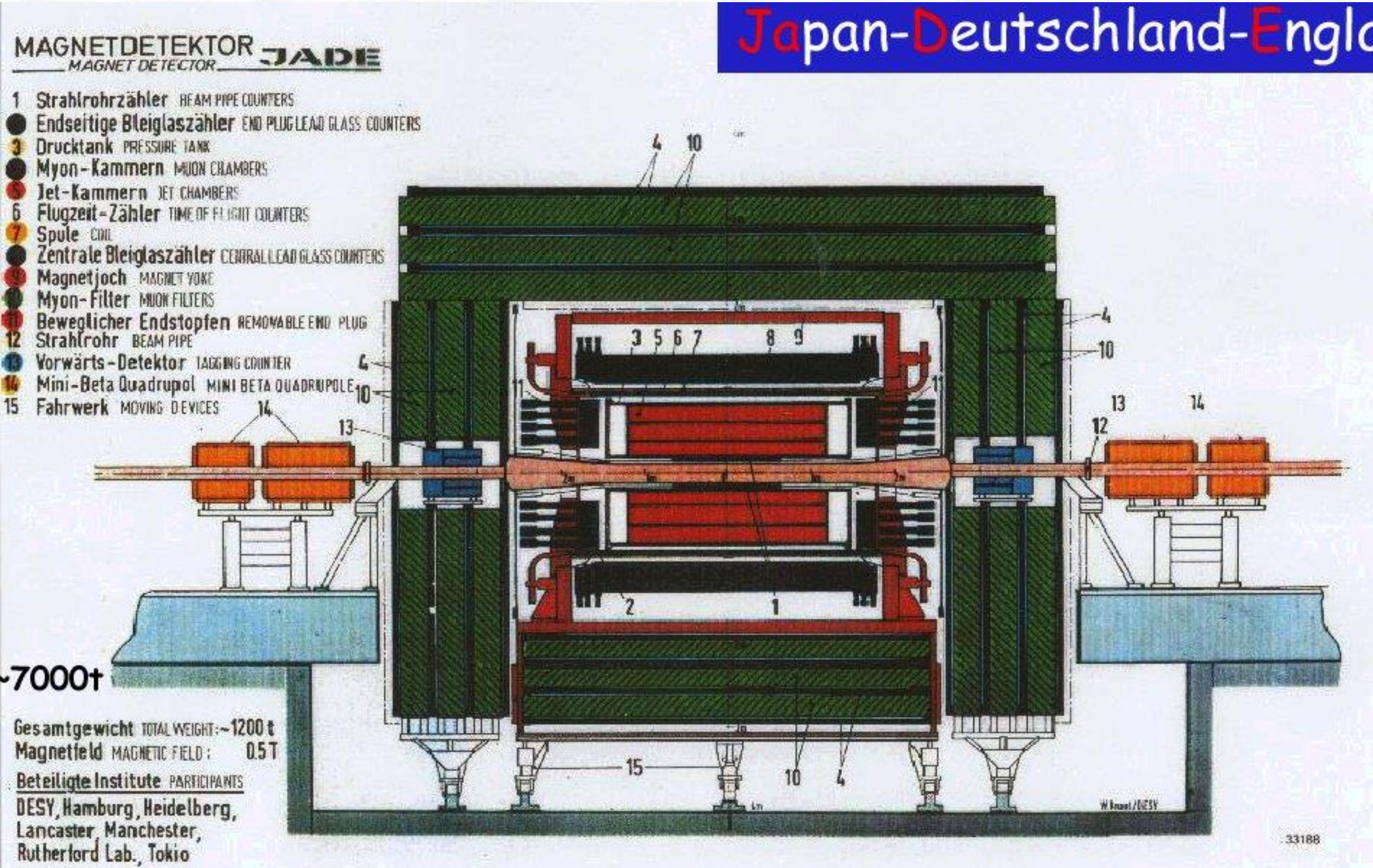

~7000t

Jet drift chamber of the OPAL experiment (CERN)

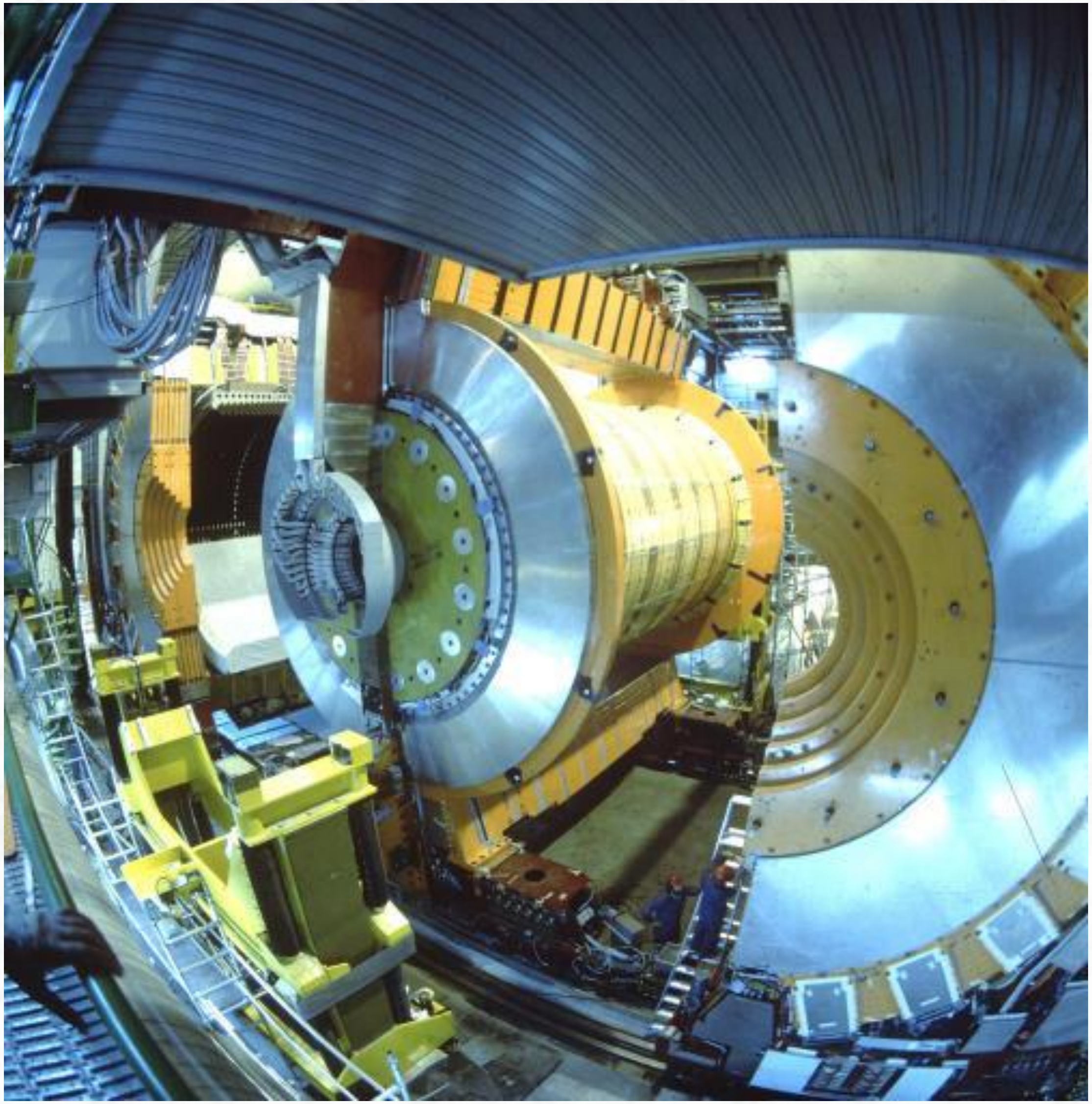

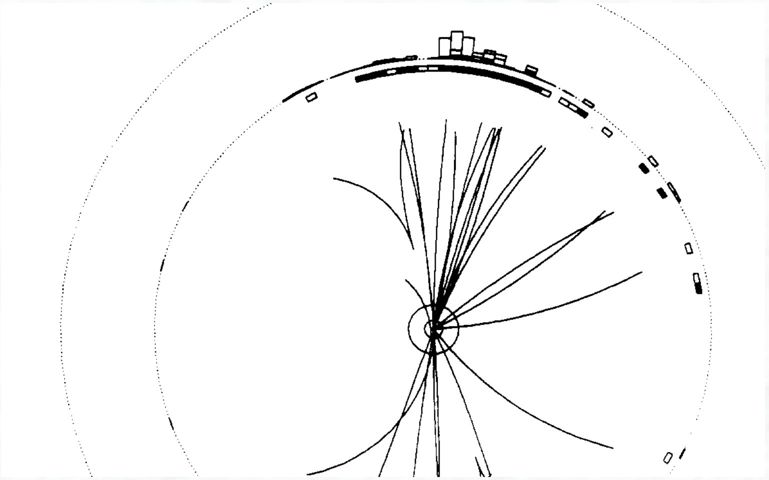

escription and operation

'he sensitive volume of the jet chamber is a c
with a length of about 4 m with conical end pl
is divided in ϕ into 24 identical sectors,
aining a sense wire plane with 159 anode wires
cathode wire planes that form the bound
'een adjacent sectors. The anode wires are loc
'een radii of 255 mm and 1835 mm, equally sp
0 mm and alternating with potential wires.
imum drift distance varies between 3 cm an
To resolve left-right ambiguities, the anode v
staggered by ± 100 μm alternately to the left
t side of the plane defined by the potential wire
matic drawing of a section of a jet chamber se

A glance in the interior of the OPAL Jet Chamber

Drift chamber of the CDF experiment (Fermilab)

A glance in the interior of the CDF drift chamber